A Pvr–AP-1–Mmp1 signaling pathway is activated in astrocytes upon traumatic brain injury

Tingting Li[1], Wenwen Shi[1], Margaret S. Ho[2,*], Yong Q. Zhang[1,*]

[1]Key Laboratory of Molecular and Developmental Biology, Institute of Genetics and Developmental Biology, University of Chinese Academy of Sciences, Chinese Academy of Sciences, Beijing 100101, China.

[2] School of Life Science and Technology, ShanghaiTech University, Shanghai, 201210, China

*Correspondence: margareth@shanghaitech.edu.cn, yqzhang@genetics.ac.cn (lead contact)

Main Points:

- The study provided RNA-seq data of astrocytes following traumatic brain injury (TBI)
- Genes involved in endocytic trafficking are upregulated in astrocytes after TBI
- A new Pvr–AP-1–Mmp1 pathway is activated in astrocytes following TBI.
- Inhibition of endocytosis in astrocytes upregulates the Pvr–AP-1–Mmp1 signaling.

Abstract

Traumatic brain injury (TBI) caused by external mechanical forces is a major health burden worldwide, but the underlying mechanism in glia remains largely unclear. We report herein that *Drosophila* adults exhibit a defective blood-brain-barrier (BBB), elevated innate immune responses, and hypertrophy of astrocytes upon consecutive strikes with a high-impact trauma device. RNA sequencing (RNA-seq) analysis of these astrocytes revealed upregulated expression of genes encoding PDGF and VEGF receptor-related (Pvr, a receptor tyrosine kinase (RTK)), adaptor protein complex 1 (AP-1, a transcription factor complex of the c-Jun N-terminal Kinase (JNK) pathway) composed of Jun-related antigen (Jra) and kayak (kay), and matrix metalloproteinase 1 (Mmp1) following TBI. Interestingly, Pvr is both required and sufficient for AP-1 and Mmp1 upregulation, while knockdown of AP-1 expression in the background of Pvr overexpression in astrocytes rescued Mmp1 upregulation upon TBI, indicating that Pvr acts as the upstream receptor for the downstream AP-1–Mmp1 transduction. Moreover, dynamin-associated endocytosis was found to be an important regulatory step in downregulating Pvr signaling. Our results identify a new Pvr–AP-1–Mmp1 signaling pathway in astrocytes in response to TBI, providing potential targets for developing new therapeutic strategies of TBI.

Keywords: TBI, astrocytes, Pvr, RNA-seq, *Drosophila*

Introduction

Traumatic brain injury (TBI) is one of the leading causes for adult disability due to limited neurological recovery (Joy et al., 2019). About 43% of people discharged after hospitalization for acute TBI develop long-term locomotor disability (Ma et al., 2014). TBI triggers primary neural injuries via rapid physical forces that damage axons, glia and blood vessels (Chodobski et al., 2011; Daneshvar et al., 2015), followed by diverse secondary damage such as Wallerian axon degeneration (Büki and Povlishock, 2006) and blood-brain barrier (BBB) dysfunction (Chodobski et al., 2011) in the central nervous system (CNS). The outcome of TBI is affected by various factors including age and diet (Byrns et al., 2021; Katzenberger et al., 2016). In addition, glial cells are critical mediators in response to TBI in the mammalian brain (Mira et al., 2021). During TBI, astrocytes become active, a process characterized by swelling, scar tissue formation, and engulfment of neuronal debris (Liddelow et al., 2017; Sofroniew and Vinters, 2010), while microglia rapidly transform to their active state to phagocytose cell debris (Davalos et al., 2005).

Drosophila melanogaster is an ideal model organism for discovering new gene networks and investigating the molecular and cellular responses to CNS injury (Ayaz et al., 2008; Bier, 2005; Hoopfer et al., 2006; MacDonald et al., 2006). *Drosophila* astrocyte-like glia (henceforth astrocytes), the conserved counterparts for mammalian astrocytes, and ensheathing glia (ENG) constitute the major glial subclasses in the CNS (Doherty et al., 2009; Stork et al., 2014). A previous study revealed that *Drosophila* ENG perform the phagocytic function by the engulfment receptor Draper which interacts with downstream signaling components, including ced-6, Shark, Src42a, c-Jun N-terminal Kinase (JNK), and Mmp1 in the glial engulfment process in response to axotomy (Awasaki et al., 2006; Doherty et al., 2014; Lu et al., 2014; Lu et al., 2017; Purice et al., 2017). Although ENG function upon axotomy has been well characterized, the response of other types of glia such as astrocytes to neural injury remains unclear.

78 In mammals, signaling by platelet-derived growth factor (PDGF) directs cell
79 migration, alters cell shape, and plays a role in wound healing (Hoch and Soriano,
80 2003; Sil et al., 2018). Meanwhile, vascular endothelial growth factor (VEGF)
81 signaling is critical for cell proliferation and survival, and vascular endothelial cell
82 mitogenesis and permeability (Apte et al., 2019; Sakurai et al., 2005). Pvr, short for
83 PDGF- and VEGF receptor-related, is the sole *Drosophila* ortholog of the PDGF and
84 VEGF receptor families (Cho et al., 2002). Pvr interacts with different signaling
85 molecules in a context-dependent manner. For example, Pvr regulates thorax closure
86 during metamorphosis via the c-Jun N-terminal Kinase (JNK) signaling pathway
87 (Ishimaru et al., 2004), but the Pvr-mediated wound-induced epidermal cell migration
88 does not depend on JNK (Wu et al., 2009). The JNK Activator Protein-1 (AP-1)
89 signaling pathway is involved in different cellular processes, including cell migration
90 (Pastor-Pareja et al., 2004), organ size control (Willsey et al., 2016), and cell death
91 (Moreno et al., 2002). The JNK effector AP-1 complex, composed of heterodimeric
92 Jun/Jun-related antigen (Jra) and Fos/kayak (kay), promotes transcription of genes
93 including matrix metalloproteinase 1 (Mmp1) that functions in tissue remodeling,
94 regulation of inflammatory processes, and metastasis of cancer cells (Egeblad and
95 Werb, 2002; Page-McCaw et al., 2007; Parks et al., 2004).
96 Previous studies have implicated a role for ensheathing glia, Draper pathway,
97 and the innate immune pathway in response to TBI (Doherty et al., 2009; Lu et al.,
98 2017; Purice et al., 2017; Katzenberger et al., 2013). However, whether astrocytes
99 also play a role in TBI response remains elusive. Herein, using a *Drosophila* TBI
100 model induced with a high-impact trauma (HIT) device (Katzenberger et al., 2013),
101 we found that TBI caused multiple defects including upregulated expression of innate
102 immune genes and astrocyte hypertrophy. To uncover the molecular pathways
103 activated by TBI, we performed RNA sequencing (RNA-seq) analysis of astrocytes
104 sorted by fluorescence-activated cell sorting (FACS) to profile TBI-induced genes.
105 Interestingly, we showed that the expression of Pvr, AP-1, and Mmp1 was upregulated

following TBI. Knockdown of Pvr or AP-1 expression in astrocytes rescued TBI-induced Mmp1 upregulation, while Pvr overexpression promoted Mmp1 expression via AP-1 upon TBI. Our findings identify a new Pvr–AP-1–Mmp1 signaling pathway that acts predominantly in astrocytes in response to TBI, and shed light on the mechanisms of astrocyte responses following TBI.

Materials and Methods:

Drosophila stocks and husbandry

Flies were maintained on standard cornmeal medium at 25°C otherwise indicated. The following *Drosophila* strains were used: w^{1118}, *UAS-mCD8::GFP*, *R86E01-Gal4* (#45914; Bloomington), *R54F03-Gal4* (#39157; Bloomington), *UAS-Redstinger* (#8547; Bloomington), *UAS-Jra* (#7216; Bloomington), *UAS-kay* (#7213; Bloomington), *UAS-Pvr* (#58429; Bloomington), *UAS-nLacZ* (#3955, Bloomington), *PCNA-GFP* (#25749; Bloomington) (Thacker et al., 2003), and *TRE-dsRed* (Chatterjee and Bohmann, 2012). *UAS-draper-RNAi*, *UAS-Pvr-RNAi*, *UAS-Jra-RNAi*, *UAS-kay-RNAi*, *UAS-Arpc2-RNAi*, *UAS-cpa-RNAi*, *UAS-cpb-RNAi*, *UAS-Stam –RNAi*, *UAS-Vps24-RNAi*, and *UAS-Chmp1-RNAi* flies were obtained from Tsinghua Fly Center (https://thfc.zzbd.org/en). *y w UAS-CD8::GFP hs-FLP; tubP-Gal80 FRT-40A/CyO; alrm-Gal4 UAS-CD8::GFP UAS-Dcr2/TM6 Tb Hu* (alrm-Gal4 is a specific driver in astrocytes (Doherty et al., 2009), a gift from Oren Schuldiner) and *FRT-40A* (a gift from Liqun Luo) were used for MARCM analysis of astrocytes. *UAS-shibire*^{ts1} (Pfeiffer et al., 2012) was provided by Y. Zhong at Tsinghua University.

Traumatic brain injury (TBI) Assay

Construction and use of the HIT device were described previously (Katzenberger et al., 2013). Deflection of the spring to 90° was the standard angle for strike. Mortality index at 24 h (MI_{24}) were determined by analyzing at least 120 flies (20 flies for each test).

134 **Dye penetration assay**

135 Dye penetration experiments were performed as previously described (Bainton et
136 al., 2005). 10 kD Texas red-conjugated dextran (Molecular Probes) at 2.5 mM was
137 injected into the soft tissue between two abdominal segments of the exoskeleton of
138 flies with and without TBI. Flies were allowed to recover in fresh food tubes and
139 photographed 2 h later on a Zeiss microscope to detect the integrity of brain-eye
140 barrier (BEB). To detect the integrity of BBB, fly brains were dissected at 2 h after
141 injection and examined under an Olympus FluoView FV1000 microscope.

142 **MARCM analysis**

143 Mosaic analysis with a repressible cell marker (MARCM) analysis in astrocytes
144 was carried out largely following previous publications (Jia et al., 2019; Lee and Luo,
145 1999). Specifically, newly laid eggs were collected for a 4–5 h interval and cultured at
146 18°C. Clones were induced by heat shock at 24 h after larval hatching in a 37°C water
147 bath for 15 min and flies were raised at 25°C after heat shock until
148 immunohistochemistry analysis of adult brain.

149 **Immunohistochemistry analysis and confocal microscopy**

150 Brain tissues were dissected out from adult after specific treatments. Fixation and
151 staining of adult brains were performed as previously described (Jia et al., 2019).
152 Brains were mounted on slides in Vectashield mounting media (Vector Labs). Primary
153 antibodies were used at the following dilutions: chicken anti-GFP (ab13970, Abcam)
154 at 1:1000, mouse anti-Repo (8D12, DSHB) at 1:100, mouse anti-Elav (9F8A9, DSHB)
155 at 1:100, mouse anti-Mmp1 (3A6B4, 3B8D12, and 5H7B11, DSHB) each at 1:20 for
156 all three antibodies, rabbit anti-Pvr (McDonald et al., 2003) at 1:1000, rabbit
157 anti-Dcp-1 (Asp216, Cell Signaling Technology (CST)) at 1:100, rabbit anti-pH3
158 (06-570, Millipore) at 1:1000, and mouse anti-β-gal (40-1a, DSHB) at 1:100. All
159 secondary antibodies (Alexa Fluor 488, 568 or 633 labeled; Molecular Probes) were
160 used at a dilution of 1:1000. The nuclei dye To-Pro-3 Iodide (T3605, ThermoFisher)
161 was also used at a dilution of 1:1000. The cell-permeant Mitotracker (M22426,

162 ThermoFisher) was used at a concentration of 100 nM. For soma diameter analysis,
163 we measured the average of long and short axes of astrocytes. All images were
164 collected using an Olympus FV1000 laser scanning confocal microscope and
165 processed with ImageJ. Serial images of 25–30 μm (one image per 1 μm slice) were
166 projected for presentation and statistical analysis.

167 **Astrocyte preparation for RNA-seq analysis**

168 Flies were collected at 3 days after eclosion and treated with TBI. Brains from
169 adult flies (*R86E01-Gal4*/*UAS-Redstinger*) with no injury, 4 h after injury and 24 h
170 after injury were dissected out in freshly prepared adult hemolymph saline (AHS)
171 buffer, as previously described (Yang et al., 2016). Briefly, a total of ~50 brains for
172 each group was immediately transferred to an Eppendorf tube (1.5 mL) containing
173 200 μL AHS with Pronase (1 mg/mL; P5147, SigmaAldrich) and Dispase (1 mg/mL;
174 LS02104, Worthington Biochemical Corporation). After tissue digestion for 30 min at
175 25°C, the enzyme medium was removed, followed by two brief, gentle washes with
176 fresh AHS containing 2% PBS. Brain samples were then triturated by gently pipetting
177 in 1 mL AHS through four fire-polished Pasteur pipettes with descending pore sizes
178 (400 μm, 300 μm, 200 μm, and 100 μm) for a total of ~20 min. Next, the dissociated
179 cells were centrifuged for 10 min at 100 × *g* and the AHS was replaced with the same
180 buffer to minimize any RNA content released from damaged cells during the
181 trituration process. Finally, dissociated tissues were filtered through 45 μm filter and
182 then put on ice. FACS sorting was performed according to the following gating
183 procedure with 70 μm nozzle by BD FACS Aria: (1) an initial SSC-A/FSC-A gate to
184 minimize debris; (2) a SSC-A/pe-Texa Ted-A gate to choose only red fluorescence
185 positive cells. At this step, 1600 cells were sorted directly into ice-cold cell lysis
186 buffer (oligo-dT_{30}VN primer, ribonuclease inhibitor, dNTP mix) and stored at −80°C
187 until all samples were ready for RNA extraction and cDNA amplification.

188 **cDNA library preparation**

189 A total of 5 biological replicates were collected for each condition (no injury, 4 h

190 after injury, and 24 h after injury). Cell samples were sent to the Anoroad Company
191 for RNA extraction. An Oligo-dT primer was introduced to the reverse transcription
192 reaction for first-strand cDNA synthesis, followed by PCR amplification to enrich the
193 cDNA and magbeads purification step was used to purify the products. Briefly,
194 Smart-Seq2 method was used to amplify cDNA. Concentration and integrity of cDNA
195 was assessed using Qubit 3.0 Flurometer (Life Technologies) and Agilent 2100
196 Bioanalyzer (Agilent Technologies) to ensure the cDNA length was around 1-2 kbp.
197 After quality control, 40 ng cDNA was used to be fragmented at 350 bp by
198 Bioruptor® Sonication System (Diagenode Inc.). To construct Illumina library, end
199 repair, 3' ends A-tailing, adaptor ligation, PCR amplification and library validation
200 were performed. PerkinElmer LabChip® GX Touch and Step OnePlus™ Real-Time
201 PCR System were used for library quality inspection. Qualified libraries were loaded
202 on Illumina Hiseq platform for PE150 sequencing.

203 **RNA-seq and data analysis.**

204 A total of 539 million reads (average 35.9 million reads per sample) was obtained.
205 The fastq data were first processed with Trimmomatic (Bolger et al., 2014) to remove
206 Illumina adaptor. The remaining data was aligned against the UCSC *D. melanogaster*
207 genome (dm6) using Hisat2 (Kim et al., 2015; Kim et al., 2019; Pertea et al., 2016)
208 with the annotation file of the same version. On average, 92% of the initial reads were
209 mapped to dm6. HTSeq was used to calculate the raw read counts of genes for each
210 sample. DESeq2 (Love et al., 2014) was used to normalize the data. Transcripts were
211 considered as significantly differentially expressed if their adjusted p values were less
212 than 0.01 ($p < 0.01$) by the Benjamini-Hochberg method. Following normalization of
213 the data, DESeq2 was used to perform pairwise comparisons between the control and
214 experimental groups using parametric tests. Genes with absolute value of logarithmic
215 fold change ($\log_2$FC) > 1.0 were qualified for the final set of DEGs. Volcano plots and
216 heatmap were constructed for visualization of the resulting expression intensity data
217 following the identification of DEGs and RNA-Seq data normalization by the

218 adjusted p value calculations.

219 **Quantitative reverse transcription-PCR analysis.**

220 RT-qPCR was performed largely based on previous protocols (Zhao et al., 2020).
221 Flies were treated with the same conditions as the RNA-seq experiment. RNA for
222 antimicrobial peptides (AMPs) analysis was extracted from whole fly brains by TriZol.
223 RNA for confirming RNA-seq findings was isolated from more than 10000 astrocytes
224 sorted by FACS using the PicoPure RNA isolation kit (KIT0204, Life Technologies).
225 cDNA was generated with SuperScript III First-Strand Synthesis SuperMix
226 (11752250, Invitrogen). For each gene, at least three pairs of qPCR primers were
227 screened by standard curve analysis, and the best primer pairs were chosen based on
228 their efficiency and specificity. Real-time qPCR was carried out by KAPA Library
229 Quantification Kit (KR0389, KAPA Biosystems). Primer sequences are provided in
230 Table S1.

231 **Thermogenetic inhibition of endocytosis**

232 For inhibition of endocytosis in astrocytes using *UAS-Shi*^{ts}, crosses were reared
233 and treated by HIT device at 23°C to avoid unintended inactivation. For
234 thermogenetic inactivation, flies after TBI were undergone intermittent temperature
235 treatment at 32°C (32°C for 30 min, and then back to 23°C for 30 min, for four
236 rounds, four hours in total) until dissection.

237 **Statistical analysis**

238 All statistical comparisons were performed using GraphPad Prism software, with
239 significance indicated by $***$ ($p \leq 0.001$), $**$ ($p \leq 0.01$), $*$ ($p \leq 0.05$), and ns ($p > 0.05$).
240 One-way ANOVA was used to compare multiple group means. Student's t-tests were
241 used for statistical comparisons between two groups.

242

243 ## Results

244 **TBI is induced in *Drosophila* adults by a high-impact trauma (HIT) device**

245 To analyze how brains respond to TBI, we applied consecutive strikes to adult

246 flies using a HIT device to induce brain injury as described previously (Katzenberger
247 et al., 2015). To quantify the degree of injury, we analyzed the mortality index at 24 h
248 after TBI (MI_{24}), defined as the percentage of dead over the total flies tested.
249 Consistent with a previous report (Katzenberger et al., 2013), MI_{24} of 3-day-old adult
250 flies was 20 ± 3.18% after 4 HIT strikes (Figure 1A). MI_{24} after 6 strikes was 71.88 ±
251 7.44%, suggesting that increasing the number of strikes results in a higher MI_{24} rate
252 (Figure 1A). Given that TBI has been shown to disrupt the formation of the
253 blood-brain barrier (BBB) in mammals and flies and blood-eye barrier (BEB) in flies
254 (Rodríguez-Baeza et al., 2003; Sangiorgi et al., 2013; Katzenberger et al., 2015;
255 Saikumar et al., 2020), we examined BBB/BEB integrity 2 h after injecting
256 tetramethylrhodamine-conjugated dextran (molecular weight = 10,000 Da) into adult
257 fly abdominal segments (Bainton et al., 2005). The dye crossed the barrier and
258 penetrated the retina and brain, indicating that both BBB and BEB were disrupted
259 after HIT strikes (Figure 1B–G). The percentage of flies exhibiting dextran-permeable
260 BBB increased as the number of strikes increased from 0 to 6, with six strikes
261 resulting in severe BBB disruption (Figure 1G) but maintaining a moderate viability
262 providing enough samples for phenotypic analysis. Based on these results, six HIT
263 strikes administered at 5 min intervals were applied to induce TBI throughout the
264 present study.

265 In addition to disruption of BBB/BEB integrity, we also analyzed TBI-induced
266 secondary damage such as local and systemic immune responses. Given that Toll and
267 immune deficiency (Imd) are the two crucial innate immune response pathways in
268 *Drosophila* (Valanne et al., 2011), and their common downstream genes encode
269 antimicrobial peptides (AMPs) that protect flies from TBI injury (Alphen et al., 2022),
270 we analyzed the expression of AMPs in adult fly brains at different time points after
271 TBI. As shown by the real-time reverse transcriptase-polymerase chain reaction
272 (RT-qPCR) results, expression of the AMP genes *AttC*, *DiptB* and *Mtk* was
273 significantly upregulated at 1 h and reached a peak at 4 h after injury (Figure 1H),

274 consistent with previous reports (Barekat et al., 2016; Katzenberger et al., 2013).
275 Taken together, these results suggest that HIT strikes induce TBI reflected by
276 BBB/BEB disruption and elevated expression of innate immune response genes.
277
278 **TBI induces neuronal but not glial apoptosis in adult fly brains**
279 Given that neurons and glia have been shown to undergo cell death during both
280 primary and secondary injury responses upon TBI in humans (Ng and Lee, 2019), we
281 performed immunostaining with an antibody against Death caspase-1 (Dcp-1), the
282 homolog of human caspase-3, to detect apoptotic cells in our TBI model. Interestingly,
283 the number of Dcp-1^{+} puncta was significantly increased in adult fly brains at 24 h
284 after TBI (Figures 1I and J), with a 2.47-fold increase compared to the number in
285 uninjured controls (Figure 1K). Furthermore, we found that almost all Dcp-1^{+} puncta
286 were co-localized with Elav rather than Repo, suggesting that neurons but not glia are
287 apoptotic (Figures 1L–M"). These results suggest that, as in mammals, TBI also
288 induces neuronal apoptosis in fruit flies.
289 In addition, we analyzed cell proliferation following TBI using an antibody
290 against phospho-histone H3 (pH3), a marker for the M stage of the cell cycle, and fly
291 lines expressing the proliferating cell nuclear antigen (PCNA) fused with GFP
292 (PCNA-GFP), a reporter for the G1-S transition of mitosis (Thacker et al., 2003). As a
293 control, 3rd instar larval brains exhibited numerous GFP^{+} and pH3^{+} cells, suggesting
294 that larval brain cells proliferate vigorously (Figures S1A–A"). Interestingly,
295 essentially no GFP^{+} or pH3^{+} cells were detected in either uninjured or TBI-treated
296 adult fly brains at various time points (Figures S1B–I). These results indicate that
297 adult fly brain cells do not divide in response to TBI, whereas neurons and glia in
298 adult vertebrate brains proliferate after nervous system injury, such as stab injury and
299 TBI (Yu and He, 2019).
300

301 **TBI leads to astrocyte activation**

302 In addition to the TBI-induced neuronal apoptosis mentioned above, glial cells
303 also become reactive after nervous system injury (Burda and Sofroniew, 2014). It has
304 been shown that ENG phagocytose neuronal debris upon axotomy (Doherty et al.,
305 2009), but whether astrocytes respond to TBI remains unknown. To explore the
306 potential role of astrocytes in the TBI response, *R86E01-GAL4* (Kremer et al., 2017),
307 an astrocyte-specific driver, was used to express *UAS-mCD8::GFP* to label astrocyte
308 plasma membrane. In uninjured fly brains, GFP intensities in the cell bodies and
309 processes of astrocytes were widely distributed throughout the brain (Figures 2A and
310 2D). While no significant change in GFP intensity was detected in brains at 4 h after
311 TBI (Figures 2B and 2D), the GFP intensity was significantly increased and the cell
312 bodies of astrocytes were significantly enlarged at 24 h after TBI in the central brain
313 region, especially in the antennal lobes (ALs) (Figures 2C and 2D). Of note, these
314 results were not affected by the presence of one or two UAS transgenes as the
315 efficiency of *R86E01-GAL4* in driving the expression of either was comparable as
316 shown by the similar GFP levels (Figures 2A–C, I, and J).

317 In mammals, the hallmarks of astrocyte activation are hypertrophy of astrocytes
318 and upregulated level of the glial fibrillary acidic protein (GFAP) (Pekny et al., 2004).
319 Given that there's no GFAP homolog in *Drosophila (*Doherty et al., 2009), we
320 examined morphological changes in astrocytes at single-cell resolution following TBI
321 by mosaic analysis with a repressible cell marker (MARCM) on adult fly brains at 3–
322 4 days after eclosion. The cell bodies of these astrocytes were located at the interface
323 between neuropil and cortex regions, or in neuropils, and their cellular processes
324 infiltrated into neuropils (Figure 2E). Interestingly, astrocytes in injured brains
325 exhibited bright and distinct GFP^+ accumulations associated with their cellular
326 processes at 24 h after TBI (Figures 2F and 2G). Quantitatively, the number of these
327 accumulations per square nanometer in the cellular processes was significantly
328 increased at 24 h after TBI; the increase in the number of accumulations might be

329 responsible for the increase in GFP intensity triggered by TBI (Figure 2G).
330 Importantly, the diameter of astrocytes cell bodies was also increased at 24 h after
331 injury (Figure 2H). Taken together, these results show that astrocytes become
332 hypertrophic and reactive in adult brains at 24 h after TBI.

333 Axotomy induces expression of injury-related proteins such as extracellular
334 proteases the matrix metalloprotease (MMP) (Purice et al., 2017). In addition to the
335 morphological changes in astrocytes, we observed upregulated expression of Mmp1
336 in TBI-treated brains (Figures 2I–J'', 2M–N'', and 2Q). These Mmp1^{+} signals were
337 colocalized with membrane-bound *mCD8::GFP* driven by the astrocytes-specific
338 driver *R86E01-GAL4* or ENG-specific driver *R56F03-GAL4* (Figures 2K, 2L, 2O, and
339 2P), suggesting that Mmp1 might be produced from both types of glia after TBI.

340

341 **Transcriptional profiling of astrocytes in adult flies reveals elevated expression of**
342 **injury-related genes upon TBI**

343 To further investigate how astrocytes respond to TBI, we analyzed transcriptional
344 changes in astrocytes by RNA-seq (Figure 3A). Due to the tiny soma and
345 morphological complexity, the analysis of a purified population of glial cells has been
346 difficult and technically challenging. We have optimized a protocol for purifying
347 astrocytes from adult Drosophila of *R86E01-Gal4>UAS-Redstinger* by
348 fluorescence-activated cell sorting (FACS) (see details in Materials and Methods). As
349 FACS removes most cell masses and RFP-negative cells, the remaining RFP^{+} cells are
350 mostly viable, as shown by MitoTracker staining, and purity was 92.96% (RFP^{+} and
351 MitoTracker^{+} cells/total cells) in uninjured brains (Figure S2 A-C'). Further analysis
352 of the RNA-seq data showed that the astrocyte markers *Eaat1* (110359 reads) and
353 *alrm* (186413 reads) were highly expressed, while *nSyb*, a neuronal marker, was
354 hardly detected (125 reads) at 4 h after TBI, verifying the purity of FACS-sorted
355 astrocytes. A principal component analysis (PCA) revealed that the variance between
356 different groups (no injury vs. 4 h and 24 h after injury) was greater than the variance

357 within groups (Figure S2D). From analysis on five biological replicates for each time
358 point (no injury, 4 h, and 24 h after injury), we obtained 539 million reads (an average
359 of 36 million reads per sample) and aligned the RNA-seq reads to the *Drosophila*
360 genome. We found that 93.67 ± 0.89% of reads mapped to the *Drosophila* genome
361 (dm6 version). Using a cutoff of ≥ 2-fold differential expression (adj. p value <0.01,
362 Benjamini-Hochberg procedure), we identified 522 and 357 genes with altered
363 expression at 4 h (416 upregulated and 106 downregulated) and 24 h (229 upregulated
364 and 128 downregulated) after injury, respectively (Figures 3B–D; Table S2).

365 Gene Ontology (GO) analysis of these upregulated genes revealed that a
366 significant proportion were associated with endosomal transport, actin cytoskeleton,
367 and wound healing (Figure S3). Furthermore, we detected upregulated expression of
368 components functioning in the innate immune response after TBI. For instance,
369 expression of the components Relish and Dif of the Toll and Imd pathways was
370 upregulated in astrocytes after TBI (Figure 3D), in agreement with a previous finding
371 that Relish is necessary for TBI-induced secondary injuries (Swanson et al., 2020). In
372 addition, expression of injury-related genes including *chic*, *Jra*, *kay, rl*, *Cad96Ca*,
373 *Idgf4*, *Stam*, *draper*, *Pvr*, *spict*, *Mmp1* and *NijA*, and receptor genes including *Pvr*,
374 *draper*, *AdoR*, *PGRP-SA*, and *NimA* were upregulated in astrocytes at 4 h or 24 h after
375 injury (Table S3). A set of endocytic trafficking genes was also identified, including
376 *Arpc1*, *Arpc2*, *cpa*, *cpb*, *Stam*, and *Chmp1*. Subsequent RT-qPCR experiments
377 confirmed the upregulation of all six genes tested at 4 h and/or 24 h after TBI (Figure
378 3E), supporting the robustness of the RNA-seq analysis. As a control, the
379 astrocytes-specific *alrm* gene showed no upregulation upon TBI by RT-qPCR and
380 RNA-seq. Taken together, these findings validate the approach of RNA-seq
381 transcription profiling in detecting genes functionally related to injury responses in
382 astrocytes following TBI.
383

384 **Pvr and AP-1 are required for the upregulation of Mmp1 after TBI**

385 Among the candidates exhibiting upregulated expression in astrocytes upon TBI,
386 three receptors (Pvr, AdoR and Draper), all acting upstream of and activating the JNK
387 pathway (Ishimaru et al., 2004; Macdonald et al., 2013; Poernbacher and Vincent,
388 2018), emerged as new factors with uncharacterized functions in astrocytes (Figure
389 3D). The *Drosophila* RNA interference (RNAi) Screening Center Integrative
390 Ortholog Prediction Tool (DIOPT) identified orthologs of these three receptors,
391 subunits of transcriptional factor AP-1 (composed of Jra and kay) of the JNK pathway,
392 Mmp1, and endocytic trafficking genes in mouse and human (Table 1) (Hu et al.,
393 2011). These proteins mediate essential injury responses in vertebrates (Borea et al.,
394 2016; Motz and Coukos, 2013; Shi et al., 2021). To examine a potential role of the
395 receptors and their downstream signaling components in astrocytes after TBI, we
396 quantified the immunostaining intensity of these proteins from projected images of
397 the whole brain (including 20-30 slices with 1 μm per slice). As our RNA-seq analysis
398 revealed elevated expression of JNK-related injury genes such as *AP-1* and *Mmp1*
399 (Figure 3D and Table 1), we analyzed the expression of Mmp1, a transcriptional target
400 of AP-1 (Purice et al., 2017), as a readout for the activity of JNK signaling in response
401 to TBI. We found that upregulated Mmp1 expression induced by TBI was potently
402 suppressed by knocking down the expression of Pvr, Jra or kay (Figures 4A–D, 4F),
403 indicating that Mmp1 upregulation is mediated by Pvr and AP-1, and predominantly
404 occurrs in astrocytes. We note that the location and intensity of Mmp1 signals are
405 variable among different individuals (Figure 4), probably because the brain damage
406 caused by HIT is not stereotypical.

407 Even though flies with Draper knockdown in astrocytes exhibited high mortality,
408 analysis of escapers indicated that Mmp1 upregulation upon TBI was not completely
409 inhibited by Draper knockdown (Figure 4E and 4F). Knockdown of the other receptor
410 AdoR in astrocytes caused a weak inhibition of AP-1 and Mmp1 upregulation (Figure
411 S4A–A", S4G–H", S4I and S4J); *TRE-dsRed* that expresses the red fluorescent protein

412 dsRed under the control of 4 × AP-1 motifs (Chatterjee and Bohmann, 2012) was used
413 as a reporter for AP-1 activity. As Pvr showed the strongest regulation on Mmp1
414 expression among the three receptors (Figure 4 and S4), we focused on the potential
415 role of Pvr in astrocytes following TBI in the present study. We observed substantial
416 Pvr expression predominantly in astrocytes as RNAi knockdown of Pvr in astrocytes
417 showed greatly reduced level of Pvr in the whole brain at 24 h after TBI (Figure S5).
418 Conversely, TBI further increased the Pvr level in brains when Pvr was overexpressed
419 under the control of *R86E01-Gal4* (Figure S5). It is noteworthy to mention that
420 although Draper expression was upregulated upon axotomy (MacDonald et al., 2006)
421 and TBI (Figure 3D), inhibiting Draper expression in astrocytes did not suppress the
422 Mmp1 upregulation after TBI (Figure 4E and 4F). Taken together, these results
423 suggest that Pvr, but not Draper, and AP-1 are required for upregulated Mmp1 in
424 astrocytes after TBI.
425
426 **Pvr positively regulates AP-1 signaling and Mmp1 expression in astrocytes after**
427 **TBI**
428 We next investigated the genetic pathway by which Pvr functions in astrocytes in
429 response to TBI. We examined the activity of AP-1 using the *in vivo* reporter
430 TRE-dsRed (Chatterjee and Bohmann, 2012). In uninjured brains, we detected low
431 TRE-dsRed levels, suggesting a basal AP-1 activity (Figure 5A–A"). Similar to Mmp1,
432 TRE-dsRed levels were robustly upregulated at 24 h after TBI, suggesting activation
433 of JNK/AP-1 signaling (Figure 5B–B"). Importantly, TBI-induced expression of
434 TRE-dsRed and Mmp1 was suppressed or further upregulated when inhibiting or
435 overexpressing Pvr expression in astrocytes, respectively (Figure 5C–F").
436 Overexpression of Jra or kay alone did not affect expression of TRE-dsRed or Mmp1
437 (Figure S4A–F", 5I and 5J), suggesting that overexpressing a single subunit of the
438 AP-1 complex is not sufficient to upregulate AP-1 activity. While Pvr overexpression
439 caused an increase in TRE-dsRed and Mmp1 expression levels, *Jra* or *kay* RNAi

440 knockdown in the background of Pvr overexpression suppressed the increase (Figure
441 5G–L), indicating that Jra and kay act downstream of Pvr to mediate the injury
442 response upon TBI. These results together show that Pvr is a receptor acting upstream
443 of AP-1 signaling that promotes Mmp1 expression during the injury response in
444 astrocytes (Figure 5M).
445
446 **Disruption of endocytosis and endocytic trafficking enhances Pvr, AP-1, and**
447 **Mmp1 upregulation upon TBI**
448 How was the Pvr signalling induced by TBI regulated? It has been shown that
449 VEGFR2 endocytosis proceeds in a clathrin-dependent manner (Simons et al., 2016).
450 During clathrin-dependent endocytosis, scission needs Cdc42-interacting protein 4
451 (Cip4) to recruit dynamin and Wiskott-Aldrich syndrome protein (WASp), the
452 activator of the Arp2/3 complex that mediates actin polymerization and promotes the
453 movement of newly-formed clathrin-coated vesicles (Brüser and Bogdan, 2017).
454 VEGFRs are transmembrane RTKs that are activated when they locate at the cell
455 membrane (Simons et al., 2016). We first investigated whether endocytosis is
456 involved in Pvr signaling upon TBI. *Shibire* (*shi*) encodes a GTPase called dynamin
457 which is responsible for fission of the vesicle from the membrane (van der Bliek and
458 Meyerowitz, 1991). We analysed the effect of endocytosis on Pvr signaling by
459 blocking the activity of dynamin with a temperature sensitive mutant, shi^{ts}, in
460 astrocytes. Interestingly, both Pvr (Figures 6A, 6B, and 6E) and TRE-dsRed (Figures
461 6C, 6D, and 6F) intensities were increased at 4 h after TBI when dynamin activity
462 was blocked at the non-permissive 32°C. As a control, expression of nLacZ under the
463 same conditions as mutated dynamin did not exhibit a significant difference in the
464 intensities of Pvr and TRE-dsRed at the permissive 23°C and the non-permissive
465 32°C after TBI (Figures 6A, 6B, 6E, and 6F). These results suggest that Pvr signaling
466 is facilitated when endocytosis is blocked.
467 In addition to Pvr, results from our transcription profiling analysis also revealed

468 upregulation of the expression of actin dynamics and endocytic trafficking genes
469 including *Arpc2*, *cpa*, and *cpb* following TBI (Tables 1 and S2). To explore whether
470 endocytic trafficking genes are involved in the injury response in astrocytes, we
471 analyzed Mmp1 and TRE-dsRed expression when inhibiting the expression of Arpc2,
472 cpa, or cpb. Interestingly, TBI-induced Mmp1 levels were further increased after
473 knockdown of each of the three (Figures 7A–D, 7O); consistently, TRE-dsRed
474 expression was also increased after knockdown of *cpa* or *cpb* (Figures 7H–K, 7P).
475 These results indicate that genes involved in endocytosis and endocytic trafficking
476 normally inhibit induction of AP-1 and Mmp1 by TBI in astrocytes.

477 In addition, we also observed upregulated expression of a set of endosomal
478 sorting genes, including *Stam*, *Chmp1*, and *Vps24* that encode components of the
479 endosomal sorting complex required for transport (ESCRT)in astrocytes in response
480 to TBI (Tables 1 and S2). These genes are implicated in the formation of intraluminal
481 vesicles (ILVs) from multivesicular bodies (MVBs). Inhibiting expression of the
482 ESCRT-0 subunit Stam and the ESCRT-III subunits Chmp1 or Vps24 in astrocytes
483 however did not result in a significant difference in Mmp1 or TRE-dsRed expression
484 levels compared with controls following TBI (Figure 7E–G, 7L-N, 7O and 7P),
485 suggesting that endosome sorting in MVB may not affect Pvr signaling activity.

486

487 **Discussion**

488 Using a previously established a *Drosophila* TBI model, we found that TBI
489 causes neuronal apoptosis, BBB/BEB disruption, and astrocyte hypertrophy.
490 Astrocytes respond to TBI by elevated Pvr expression, which in turn enhances the
491 expression of the downstream effectors AP-1 and Mmp1. Our findings identify a new
492 signaling pathway upregulated in astrocytes following TBI.

493 Unlike vertebrates, in which astrocytes become reactive (reactive astrogliosis)
494 and actively clear neuronal and synaptic debris via phagocytosis upon axon injury
495 (Liddelow and Barres, 2017), axon transection in *Drosophila* shows no immediate

496 astrocytic response to injury (Doherty et al., 2009; Purice et al., 2017). Instead,
497 *Drosophila* ENG express key components of the phagocytic machinery and engulf
498 neuronal debris in response to axotomy (Doherty et al., 2009). Here, we examined for
499 the first time the molecular and cellular changes of astrocytes after TBI. Although no
500 astrocytes-mediated phagocytosis was detected upon axotomy (Doherty et al., 2009)
501 and TBI (Figure S6), astrocytes exhibited apparent damage response including
502 enlarged soma (hypertrophy) and altered cellular processes containing more
503 membrane-bound GFP^+ accumulations (Figure 2A–J). These findings suggest that
504 astrocytes are activated upon TBI, demonstrating a critical role for astrocytes in the
505 injury response.

506 The innate immune response in *Drosophila* relies on the activation of multiple
507 signaling pathways including NF-κB/Relish-mediated Imd and Doral/Dif-mediated
508 Toll signaling pathways. Interestingly, our RNA-seq data revealed elevated expression
509 of genes *Relish* and *Dif* in both pathways upon TBI (Figure 3D). However, the
510 expressions of *AMPs* were minimum in astrocytes before TBI and no AMPs genes
511 were identified in differentially expressed genes. Thus, AMPs genes were not
512 activated in astrocytes, though upregulated *AMP* expressions were detected by bulk
513 RNA-seq after TBI. In addition, expression of AP-1 (composed of Jra and kay) and
514 Mmp1 was also upregulated, indicating that the AP-1signaling pathway is activated in
515 astrocytes following TBI. Even though upregulated Mmp expression in reactive glial
516 responses is an evolutionarily conserved feature of *Drosophila* and mammalian glia
517 (Cunningham et al., 2005; Purice et al., 2017), transmembrane receptors on astrocytes
518 that regulate Mmp1 expression have not been identified. In mammals, knockdown of
519 VEGF signaling in keratinocytes reduced angiogenesis and delayed wound healing
520 (Rossiter et al., 2004). In *Drosophila,* studies of wound healing showed that Pvr likely
521 acts upstream of actin regulatory proteins that promote actin polymerization to lead
522 cells migration (Brock et al., 2012; Wu et al., 2009).

523 Through a combination of RNA-seq and genetic analyses, we identified Pvr as a

524 new receptor in astrocytes; Pvr promotes Mmp1 expression via the transcription
525 factor complex AP-1. At present, we do not know how Pvr promotes expression of
526 AP-1 and Mmp1. But previous findings show that Pvr phosphorylates JNK to trigger
527 the downstream signaling containing AP-1 during thorax closure in metamorphosis
528 (Ishimaru et al., 2004). During development, the midline glia survival and migration
529 are regulated by the ventral unpaired median (VUM) and the midline precursor 1
530 (MP1) midline neurons, the sources of Pvr ligands, i.e., PDGF- and VEGF-related
531 factor 1-3 (Pvf1-3) (Learte et al., 2008). Additionally, epidermal cell-derived Pvf1
532 may be sequestered in the blood and exposed upon injury to bind Pvr receptors on
533 wound-edge epidermal cells and initiate the extension of cell processes into the
534 wound gap (Wu et al., 2009). Specifically, Pvr ligands bind to Pvr receptor to induce
535 autophosphorylation of tyrosine residues, leading to JNK phosphorylation.
536 Phosphorylated JNK (Bsk) then phosphorylates Jun/Jra transcription factors,
537 triggering Jun/Jra association with Fos/kay, to form the AP-1 complex (Bogoyevitch
538 and Kobe, 2006). In addition, glial AP-1 is essential for recovery, ensuring brain
539 integrity and animal survival in the early post-TBI period (Byrns et al., 2021). Given
540 that Pvr and AP-1 genetically interact in astrocytes upon TBI, it is likely that Pvr acts
541 upstream of AP-1 and regulates its activity via JNK phosphorylation following brain
542 injury. We speculate that Pvr ligands that may secret from injured cells to activate
543 Pvr-positive astrocytes after TBI; activated Pvr then increases Mmp1 expression via
544 AP-1 and secretion to the intercellular space to participate in injury response.

545 In addition to Pvr, our RNA-seq data also identified other receptors potentially
546 functioning in astrocytes in response to TBI. Specifically, AdoR expression was
547 upregulated after TBI (Table S2), and knockdown of AdoR expression in astrocytes
548 led to inhibition of AP-1 after TBI (Figure S4G–J), though at a weaker extent
549 compared with Pvr knockdown. In mammals, $A_{2B}R$, a subtype of AdoR, was shown to
550 stimulate VEGF production in various cell types (Borea et al., 2016). Pvr promotes
551 the expression of adenosine deaminase-related growth factor A (Adgf-A) which

552 inactivates extracellular adenosine, the ligand of AdoR (Zurovec et al., 2002).
553 Furthermore, Pvr and AdoR collaborate in differentiating cells to maintain the
554 expression of Adgf-A (Mondal et al., 2011). Thus, it is possible that Pvr and AdoR act
555 independently or in a coordinated manner to regulate the injury response to TBI in
556 astrocytes in *Drosophila*.

557 Our RNA-seq profiling also revealed upregulation of Draper. Previous studies
558 revealed a role for Draper-mediated phagocytosis of axonal debris in ENG after
559 axotomy (Lu et al., 2017; MacDonald et al., 2006); axotomy induces Wallerian-like
560 degeneration (Büki and Povlishock, 2006; Tang-Schomer et al., 2010). Specifically,
561 damage-associated molecular pattern (DAMP) proteins released from injured neurons
562 bind to Draper and activate the JNK and JAK/STAT pathways in ENG (Doherty et al.,
563 2014; Freeman, 2015; MacDonald et al. 2013). Here, our findings showed that Draper
564 does not affect Mmp1 expression in astrocytes upon TBI. Although an increase in
565 Draper expression was detected in astrocytes by RNA-seq, knockdown of its
566 expression did not significantly suppress Mmp1 upregulation after TBI. Thus, Draper
567 activates JNK/AP-1 and JAK/STAT signaling in ENG in response to axotomy
568 (Doherty et al., 2014; MacDonald et al. 2013), whereas astrocytes respond to TBI via
569 Pvr-mediated AP-1 signaling. Despite different pathways are activated in different
570 types of glia upon brain injury, they may cooperate in response to TBI.

571 Endocytosis and trafficking of VEGFR, the mammalian Pvr homolog, regulate
572 the specificity as well as the duration and strength of the signaling output (Simons et
573 al., 2016). Once activated on the plasma membrane and translocated into the
574 cytoplasm, VEGFRs are either shuttled to lysosomes for degradation or recycled back
575 to the plasm membrane to replenish the receptor pool (Simons et al., 2016). Our
576 findings showed that disruption of endocytosis by disrupting dynamin activity and
577 inhibiting the expression of Arpc2, cpa, or cpb that regulate endocytic transport into
578 early endosomes enhanced the AP-1 and Mmp1 upregulation in astrocyte following
579 TBI (Figures 7A–D, 7H–K, 7O, 7P). As receptor endocytosis attenuates the strength

580 or duration of many signaling processes by physically reducing the concentration of
581 cell surface receptors accessible to the ligand (Jékely et al., 2005), blocking
582 dynamin-mediated endocytosis and endocytic trafficking potentially results in
583 accumulated Pvr receptors on the plasma membrane to activate the downstream
584 effector AP-1, thereby enhancing the astrocytes response to TBI. On the other hand,
585 ubiquitinated RTKs are recognized by ESCRT-0, followed by sequential recruitment
586 of ESCRT-I, ESCRT-II, and ESCRT-III onto the membranes of MVBs to form
587 intraluminal vesicles (ILVs) (Goh and Sorkin, 2013). Knockdown of the ESCRT-0
588 subunit Stam and the ESCRT-III subunits Chmp1 and Vps24 did not affect the
589 expression of Pvr downstream signaling components (Figure 7E–G, 7L–N, 7O and
590 7P), suggesting that Pvr signal transduction was not regulated by endosomal sorting.

591 Considering the importance of VEGF signaling in a variety of cellular processes,
592 including wound repair (Folkman and Klagsbrun, 1987), elucidating the downstream
593 signaling mechanisms, as well as defining the full array of Pvr targets in healthy and
594 diseased brains, will be critical for dissecting the protective or detrimental roles of
595 VEGF in the context of brain injury. Given that the Pvr receptor, AP-1, and the MMP
596 family of secreted proteases are all highly conserved across species, our work
597 provides new insights into how VEGF signaling in glia mechanistically contributes to
598 the TBI response in mammals.

599

600 **Acknowledgements**

601 This work was supported in part by the Ministry of Science and Technology of China
602 (2019YFA0707100 and 2021ZD0203900 to Y.Q. Zhang), the National Natural Science
603 Foundation of China (31921002, 31830036, and 31861143031 to Y.Q. Zhang, and
604 31871039 and 32170962 to M. Ho), and the Chinese Academy of Sciences Strategic
605 Priority Research Program B grants (XDBS1020100 to Y.Q. Zhang). We thank
606 Bloomington and Tsinghua stock centers for providing fly stocks. We are also grateful

607 to Zhiguo Ma, Oren Schuldiner, Sean Speese, Yong Zhang, Zhiyong Liu, and the
608 members of the Yong Q. Zhang lab for discussion and suggestions.
609

610 **References**

611 Apte, R. S., Chen, D. S., Ferrara, N. (2019). VEGF in Signaling and Disease: Beyond
612 Discovery and Development. *Cell*, *176*(6), 1248-1264.
613 Awasaki, T., Tatsumi, R., Takahashi, K., Arai, K., Nakanishi, Y., Ueda, R., Ito, K.
614 (2006). Essential role of the apoptotic cell engulfment genes draper and ced-6 in
615 programmed axon pruning during Drosophila metamorphosis. *Neuron*, *50*(6),
616 855-867.
617 Ayaz, D., Leyssen, M., Koch, M., Yan, J., Srahna, M., Sheeba, V., Hassan, B. A.
618 (2008). Axonal injury and regeneration in the adult brain of Drosophila. *Journal of*
619 *Neuroscience*, *28*(23), 6010-6021.
620 Bainton, R. J., Tsai, L. T., Schwabe, T., DeSalvo, M., Gaul, U., Heberlein, U. (2005).
621 moody encodes two GPCRs that regulate cocaine behaviors and blood-brain barrier
622 permeability in Drosophila. *Cell*, *123*(1), 145-156.
623 Barekat, A., Gonzalez, A., Mauntz, R. E., Kotzebue, R. W., Molina, B.,
624 El-Mecharrafie, N., Ratliff, E. P. (2016). Using Drosophila as an integrated model to
625 study mild repetitive traumatic brain injury. *Sci Rep*, *6*, 25252.
626 Bier, E. (2005). Drosophila, the golden bug, emerges as a tool for human genetics.
627 *Nature Reviews. Genetics*, *6*(1), 9-23.
628 Bogoyevitch, M. A., Kobe, B. (2006). Uses for JNK: the many and varied substrates
629 of the c-Jun N-terminal kinases. *Microbiology and Molecular Biology Reviews*, *70*(4),
630 1061-1095.
631 Bolger, A. M., Lohse, M., Usadel, B. (2014). Trimmomatic: a flexible trimmer for
632 Illumina sequence data. *Bioinformatics*, *30*(15), 2114-2120.
633 Borea, P. A., Gessi, S., Merighi, S., Varani, K. (2016). Adenosine as a Multi-Signaling
634 Guardian Angel in Human Diseases: When, Where and How Does it Exert its

635 Protective Effects? *Trends in Pharmacological Sciences*, *37*(6), 419-434.
636 Brock, A. R., Wang, Y., Berger, S., Renkawitz-Pohl, R., Han, V. C., Wu, Y., Galko, M.
637 J. (2012). Transcriptional regulation of Profilin during wound closure in Drosophila
638 larvae. *Journal of Cell Science*, *125*(Pt 23), 5667-5676.
639 Brüser, L., Bogdan, S. (2017). Adherens Junctions on the Move-Membrane
640 Trafficking of E-Cadherin. *Cold Spring Harbor Perspectives in Biology*, *9*(3).
641 Büki, A., Povlishock, J. T. (2006). All roads lead to disconnection?--Traumatic axonal
642 injury revisited. *Acta Neurochirurgica*, *148*(2), 181-193; discussion 193-184.
643 Burda, J. E., Sofroniew, M. V. (2014). Reactive gliosis and the multicellular response
644 to CNS damage and disease. *Neuron*, *81*(2), 229-248.
645 Byrns C. N., Saikumar J., Bonini N. M. (2021). Glial AP1 is activated with aging and
646 accelerated by traumatic brain injury. *Nat. Aging*, *1*(7), 585-597.
647 Chatterjee, N., Bohmann, D. (2012). A versatile ΦC31 based reporter system for
648 measuring AP-1 and Nrf2 signaling in Drosophila and in tissue culture. *PLoS ONE*,
649 *7*(4), e34063.
650 Cho, N. K., Keyes, L., Johnson, E., Heller, J., Ryner, L., Karim, F., Krasnow, M. A.
651 (2002). Developmental control of blood cell migration by the Drosophila VEGF
652 pathway. *Cell*, *108*(6), 865-876.
653 Chodobski, A., Zink, B. J., Szmydynger-Chodobska, J. (2011). Blood-brain barrier
654 pathophysiology in traumatic brain injury. *Transl Stroke Res*, *2*(4), 492-516.
655 Cunningham, L. A., Wetzel, M., Rosenberg, G. A. (2005). Multiple roles for MMPs
656 and TIMPs in cerebral ischemia. *Glia*, *50*(4), 329-339.
657 Daneshvar, D. H., Goldstein, L. E., Kiernan, P. T., Stein, T. D., McKee, A. C. (2015).
658 Post-traumatic neurodegeneration and chronic traumatic encephalopathy. *Molecular*
659 *and Cellular Neurosciences*, *66*(Pt B), 81-90.
660 Davalos, D., Grutzendler, J., Yang, G., Kim, J. V., Zuo, Y., Jung, S., Gan, W. B. (2005).
661 ATP mediates rapid microglial response to local brain injury in vivo. *Nature*
662 *Neuroscience*, *8*(6), 752-758.

663 Doherty, J., Logan, M. A., Tasdemir, O. E., Freeman, M. R. (2009). Ensheathing glia
664 function as phagocytes in the adult Drosophila brain. *Journal of Neuroscience*, *29*(15),
665 4768-4781.
666 Doherty, J., Sheehan, A. E., Bradshaw, R., Fox, A. N., Lu, T. Y., Freeman, M. R.
667 (2014). PI3K signaling and Stat92E converge to modulate glial responsiveness to
668 axonal injury. *PLoS Biology*, *12*(11), e1001985.
669 Egeblad, M., Werb, Z. (2002). New functions for the matrix metalloproteinases in
670 cancer progression. *Nature Reviews. Cancer*, *2*(3), 161-174.
671 Folkman, J., Klagsbrun, M. (1987). Angiogenic factors. *Science*, *235*(4787), 442-447.
672 Freeman, M. R. (2015). Drosophila Central Nervous System Glia. *Cold Spring*
673 *Harbor Perspectives in Biology*, *7*(11).
674 Goh, L. K., Sorkin, A. (2013). Endocytosis of receptor tyrosine kinases. *Cold Spring*
675 *Harbor Perspectives in Biology*, *5*(5), a017459.
676 Hoch, R. V., Soriano, P. (2003). Roles of PDGF in animal development. *Development*,
677 *130*(20), 4769-4784.
678 Hoopfer, E. D., McLaughlin, T., Watts, R. J., Schuldiner, O., O'Leary, D. D., Luo, L.
679 (2006). Wlds protection distinguishes axon degeneration following injury from
680 naturally occurring developmental pruning. *Neuron*, *50*(6), 883-895.
681 Hu, Y., Flockhart, I., Vinayagam, A., Bergwitz, C., Berger, B., Perrimon, N., Mohr, S.
682 E. (2011). An integrative approach to ortholog prediction for disease-focused and
683 other functional studies. *BMC Bioinformatics*, *12*, 357.
684 Ishimaru, S., Ueda, R., Hinohara, Y., Ohtani, M., Hanafusa, H. (2004). PVR plays a
685 critical role via JNK activation in thorax closure during Drosophila metamorphosis.
686 *EMBO Journal*, *23*(20), 3984-3994.
687 Jékely, G., Sung, H. H., Luque, C. M., Rørth, P. (2005). Regulators of endocytosis
688 maintain localized receptor tyrosine kinase signaling in guided migration.
689 *Developmental Cell*, *9*(2), 197-207.
690 Jia, M., Meng, D., Chen, M., Li, T., Zhang, Y. Q., Yao, A. (2019). Drosophila

691 homolog of the intellectual disability-related long-chain acyl-CoA synthetase 4 is
692 required for neuroblast proliferation. *J Genet Genomics*, *46*(1), 5-17.
693 Joy, M. T., Ben Assayag, E., Shabashov-Stone, D., Liraz-Zaltsman, S., Mazzitelli, J.,
694 Arenas, M., Carmichael, S. T. (2019). CCR5 Is a Therapeutic Target for Recovery
695 after Stroke and Traumatic Brain Injury. *Cell*, *176*(5), 1143-1157.e1113.
696 Katzenberger, R. J., Chtarbanova, S., Rimkus, S. A., Fischer, J. A., Kaur, G., Seppala,
697 J. M., Wassarman, D. A. (2015). Death following traumatic brain injury in Drosophila
698 is associated with intestinal barrier dysfunction. *Elife*, *4*.
699 Katzenberger, R. J., Ganetzky, B., Wassarman, D. A. (2016). Age and diet affect
700 genetically separable secondary injuries that cause acute mortality following
701 traumatic brain injury in Drosophila. *G3 (Bethesda)*, *6*(12), 4151-66.
702 Katzenberger, R. J., Loewen, C. A., Wassarman, D. R., Petersen, A. J., Ganetzky, B.,
703 Wassarman, D. A. (2013). A Drosophila model of closed head traumatic brain injury.
704 *Proceedings of the National Academy of Sciences of the United States of America*,
705 *110*(44), E4152-4159. Kim, D., Langmead, B., Salzberg, S. L. (2015). HISAT: a fast
706 spliced aligner with low memory requirements. *Nature Methods*, *12*(4), 357-360.
707 Kim, D., Paggi, J. M., Park, C., Bennett, C., Salzberg, S. L. (2019). Graph-based
708 genome alignment and genotyping with HISAT2 and HISAT-genotype. *Nature*
709 *Biotechnology*, *37*(8), 907-915.
710 Kremer, M. C., Jung, C., Batelli, S., Rubin, G. M., Gaul, U. (2017). The glia of the
711 adult Drosophila nervous system. *Glia*, *65*(4), 606-638.
712 Learte, A. R., Forero, M. G., Hidalgo, A. (2008). Gliatrophic and gliatropic roles of
713 PVF/PVR signaling during axon guidance. *Glia*, *56*(2), 164-176.
714 Lee, T., Luo, L. (1999). Mosaic analysis with a repressible cell marker for studies of
715 gene function in neuronal morphogenesis. *Neuron*, *22*(3), 451-461.
716 Liddelow, S. A., Barres, B. A. (2017). Reactive Astrocytes: Production, Function, and
717 Therapeutic Potential. *Immunity*, *46*(6), 957-967.
718 Liddelow, S. A., Guttenplan, K. A., Clarke, L. E., Bennett, F. C., Bohlen, C. J.,

719 Schirmer, L., Barres, B. A. (2017). Neurotoxic reactive astrocytes are induced by
720 activated microglia. *Nature*, *541*(7638), 481-487.
721 Love, M. I., Huber, W., Anders, S. (2014). Moderated estimation of fold change and
722 dispersion for RNA-seq data with DESeq2. *Genome Biology*, *15*(12), 550.
723 Lu, T. Y., Doherty, J., Freeman, M. R. (2014). DRK/DOS/SOS converge with
724 Crk/Mbc/dCed-12 to activate Rac1 during glial engulfment of axonal debris. *Proc.*
725 *Natl. Acad. Sci. USA*, *111*(34), 12544-12549.
726 Lu, T. Y., MacDonald, J. M., Neukomm, L. J., Sheehan, A. E., Bradshaw, R., Logan,
727 M. A., Freeman, M. R. (2017). Axon degeneration induces glial responses through
728 Draper-TRAF4-JNK signaling. *Nature Communications*, *8*, 14355.
729 Ma, V. Y., Chan, L., Carruthers, K. J. (2014). Incidence, prevalence, costs, and impact
730 on disability of common conditions requiring rehabilitation in the United States:
731 stroke, spinal cord injury, traumatic brain injury, multiple sclerosis, osteoarthritis,
732 rheumatoid arthritis, limb loss, and back pain. *Archives of Physical Medicine and*
733 *Rehabilitation*, *95*(5), 986-995.e981.
734 MacDonald, J. M., Beach, M. G., Porpiglia, E., Sheehan, A. E., Watts, R. J., Freeman,
735 M. R. (2006). The Drosophila cell corpse engulfment receptor Draper mediates glial
736 clearance of severed axons. *Neuron*, *50*(6), 869-881.
737 Macdonald, J. M., Doherty, J., Hackett, R., Freeman, M. R. (2013). The c-Jun kinase
738 signaling cascade promotes glial engulfment activity through activation of draper and
739 phagocytic function. *Cell Death and Differentiation*, *20*(9), 1140-1148.
740 McDonald, J. A., Pinheiro, E. M., Montell, D. J. (2003). PVF1, a PDGF/VEGF
741 homolog, is sufficient to guide border cells and interacts genetically with Taiman.
742 *Development*, *130*(15), 3469-3478.
743 Mira, R. G., Lira, M., Cerpa, W. (2021). Traumatic Brain Injury: Mechanisms of Glial
744 Response. *Front Physiol*, *12*, 740939.
745 Mondal, B. C., Mukherjee, T., Mandal, L., Evans, C. J., Sinenko, S. A.,
746 Martinez-Agosto, J. A., Banerjee, U. (2011). Interaction between differentiating cell-

747 and niche-derived signals in hematopoietic progenitor maintenance. *Cell*, *147*(7),
748 1589-1600.
749 Moreno, E., Yan, M., Basler, K. (2002). Evolution of TNF signaling mechanisms:
750 JNK-dependent apoptosis triggered by Eiger, the Drosophila homolog of the TNF
751 superfamily. *Current Biology*, *12*(14), 1263-1268.
752 Motz, G. T., Coukos, G. (2013). Deciphering and reversing tumor immune
753 suppression. *Immunity*, *39*(1), 61-73. https://doi.org/10.1016/j.immuni.2013.07.005
754 Ng, S. Y., & Lee, A. Y. W. (2019). Traumatic Brain Injuries: Pathophysiology and
755 Potential Therapeutic Targets. *Front Cell Neurosci*, *13*, 528.
756 Page-McCaw, A., Ewald, A. J., Werb, Z. (2007). Matrix metalloproteinases and the
757 regulation of tissue remodelling. *Nature Reviews. Molecular Cell Biology*, *8*(3),
758 221-233.
759 Parks, W. C., Wilson, C. L., López-Boado, Y. S. (2004). Matrix metalloproteinases as
760 modulators of inflammation and innate immunity. *Nature Reviews. Immunology*, *4*(8),
761 617-629.
762 Pastor-Pareja, J. C., Grawe, F., Martín-Blanco, E., García-Bellido, A. (2004). Invasive
763 cell behavior during Drosophila imaginal disc eversion is mediated by the JNK
764 signaling cascade. *Developmental Cell*, *7*(3), 387-399.
765 Pekny M, Pekna M. (2004). Astrocyte intermediate filaments in CNS pathologies and
766 regeneration. *The Journal of Pathology, 204*(4):428-37.
767 Pertea, M., Kim, D., Pertea, G. M., Leek, J. T., Salzberg, S. L. (2016). Transcript-level
768 expression analysis of RNA-seq experiments with HISAT, StringTie and Ballgown.
769 *Nature Protocols*, *11*(9), 1650-1667.
770 Pfeiffer, B. D., Truman, J. W., Rubin, G. M. (2012). Using translational enhancers to
771 increase transgene expression in Drosophila. *Proceedings of the National Academy of*
772 *Sciences of the United States of America, 109*(17), 6626-6631.
773 Poernbacher, I., Vincent, J. P. (2018). Epithelial cells release adenosine to promote
774 local TNF production in response to polarity disruption. *Nature Communications*, *9*(1),

4675.

Purice, M. D., Ray, A., Munzel, E. J., Pope, B. J., Park, D. J., Speese, S. D., Logan, M. A. (2017). A novel Drosophila injury model reveals severed axons are cleared through a Draper/MMP-1 signaling cascade. *Elife*, *6*.

Rodríguez-Baeza, A., Reina-de la Torre, F., Poca, A., Martí, M., Garnacho, A. (2003). Morphological features in human cortical brain microvessels after head injury: a three-dimensional and immunocytochemical study. *Anatomical Record. Part A, Discoveries in Molecular, Cellular, and Evolutionary Biology*, *273*(1), 583-593.

Rossiter, H., Barresi, C., Pammer, J., Rendl, M., Haigh, J., Wagner, E. F., Tschachler, E. (2004). Loss of vascular endothelial growth factor a activity in murine epidermal keratinocytes delays wound healing and inhibits tumor formation. *Cancer Research*, *64*(10), 3508-3516.

Saikumar J, Byrns C. N., Hemphill M., Meaney D. F., Bonini N. M. (2020). Dynamic neural and glial responses of a head-specific model for traumatic brain injury in Drosophila. *Proceedings of the National Academy of Sciences of the United States of America*, 117(29):17269-77.

Sakurai, Y., Ohgimoto, K., Kataoka, Y., Yoshida, N., Shibuya, M. (2005). Essential role of Flk-1 (VEGF receptor 2) tyrosine residue 1173 in vasculogenesis in mice. *Proceedings of the National Academy of Sciences of the United States of America*, *102*(4), 1076-1081.

Sangiorgi, S., De Benedictis, A., Protasoni, M., Manelli, A., Reguzzoni, M., Cividini, A., Balbi, S. (2013). Early-stage microvascular alterations of a new model of controlled cortical traumatic brain injury: 3D morphological analysis using scanning electron microscopy and corrosion casting. *Journal of Neurosurgery*, *118*(4), 763-774.

Shi, X., Luo, L., Wang, J., Shen, H., Li, Y., Mamtilahun, M., Yang, G. Y. (2021). Stroke subtype-dependent synapse elimination by reactive gliosis in mice. *Nature Communications*, *12*(1), 6943.

Sil, S., Periyasamy, P., Thangaraj, A., Chivero, E. T., Buch, S. (2018). PDGF/PDGFR

803 axis in the neural systems. *Molecular Aspects of Medicine*, *62*, 63-74.
804 Simons, M., Gordon, E., Claesson-Welsh, L. (2016). Mechanisms and regulation of
805 endothelial VEGF receptor signaling. *Nature Reviews. Molecular Cell Biology*, *17*(10),
806 611-625.
807 Sofroniew, M. V., Vinters, H. V. (2010). Astrocytes: biology and pathology. *Acta*
808 *Neuropathologica*, *119*(1), 7-35.
809 Stork, T., Sheehan, A., Tasdemir-Yilmaz, O. E., Freeman, M. R. (2014). Neuron-glia
810 interactions through the Heartless FGF receptor signaling pathway mediate
811 morphogenesis of Drosophila astrocytes. *Neuron*, *83*(2), 388-403.
812 Swanson, L. C., Trujillo, E. A., Thiede, G. H., Katzenberger, R. J., Shishkova, E.,
813 Coon, J. J., Ganetzky, B., Wassarman, D. A. (2020). Survival following traumatic
814 brain injury in Drosophila is increased by heterozygosity for a mutation of the
815 NF-kappaB innate immune response transcription factor Relish. *Genetics*, *216*(4),
816 1117-1136.
817 Tang-Schomer, M. D., Patel, A. R., Baas, P. W., Smith, D. H. (2010). Mechanical
818 breaking of microtubules in axons during dynamic stretch injury underlies delayed
819 elasticity, microtubule disassembly, and axon degeneration. *FASEB Journal*, *24*(5),
820 1401-1410.
821 Thacker, S. A., Bonnette, P. C., Duronio, R. J. (2003). The contribution of
822 E2F-regulated transcription to Drosophila PCNA gene function. *Current Biology*,
823 *13*(1), 53-58.
824 Valanne, S., Wang, J. H., Rämet, M. (2011). The Drosophila Toll signaling pathway.
825 *Journal of Immunology*, *186*(2), 649-656.
826 Van Alphen B., Stewart S., Iwanaszko M., Xu F, Li K., Rozenfeld S., Ramakrishnan
827 A., Itoh T. Q., Sisobhan S., Qin Z. et al., (2022). Glial immune-related pathways
828 mediate effects of closed head traumatic brain injury on behavior and lethality in
829 Drosophila. *PLoS Biololy*, *20*(1), e3001456.
830 Willsey, H. R., Zheng, X., Carlos Pastor-Pareja, J., Willsey, A. J., Beachy, P. A., Xu, T.

(2016). Localized JNK signaling regulates organ size during development. *Elife*, *5*.

A. M. van der Bliek, E. M. Meyerowitz (1991). Dynamin-like protein encoded by the Drosophila shibire gene associated with vesicular traffic. *Nature, 351*(6325), 411-414.

Wu, Y., Brock, A. R., Wang, Y., Fujitani, K., Ueda, R., Galko, M. J. (2009). A blood-borne PDGF/VEGF-like ligand initiates wound-induced epidermal cell migration in Drosophila larvae. *Current Biology*, *19*(17), 1473-1477.

Yang, C. P., Fu, C. C., Sugino, K., Liu, Z., Ren, Q., Liu, L. Y., Lee, T. (2016). Transcriptomes of lineage-specific Drosophila neuroblasts profiled by genetic targeting and robotic sorting. *Development*, *143*(3), 411-421.

Yu, S., He, J. (2019). Stochastic cell-cycle entry and cell-state-dependent fate outputs of injury-reactivated tectal radial glia in zebrafish. *Elife*, *8*.

Zhao, K., Hong, H., Zhao, L., Huang, S., Gao, Y., Metwally, E., Zhang, Y. Q. (2020). Postsynaptic cAMP signaling regulates the antagonistic balance of Drosophila glutamate receptor subtypes. *Development*, *147*(24).

Zurovec, M., Dolezal, T., Gazi, M., Pavlova, E., Bryant, P. J. (2002). Adenosine deaminase-related growth factors stimulate cell proliferation in Drosophila by depleting extracellular adenosine. *Proceedings of the National Academy of Sciences of the United States of America*, *99*(7), 4403-4408.

850 ## Figure legends

851 **Figure 1. TBI is induced in adult flies by a high impact trauma (HIT) device.**

852 (A) MI_{24} is the mortality index calculated from the percentage of dead over total flies.
853 Increasing the number of strikes from 4 to 6 increases the MI_{24} value. Error bars
854 denote standard error of the mean (SEM; ***p <0.001, Student's t-test). (B–E) The
855 intactness of blood-eye-barrier (BEB) and blood-brain-barrier (BBB) before or after 6
856 strikes is indicated by the accumulated fluorescence intensity at the border of the eye
857 (B, D) and brain (C, E), respectively. The examination was carried out at 2 h after
858 fluorescent dye injection. Arrows indicate the hemolymph exclusion line. Scale bar =
859 100 μm. (F) The percentage of permeable BEB with or without TBI (***p <0.001).
860 (G) The percentage of permeable BBB following different numbers of strikes. Error
861 bars denote SEM (**p <0.01 and ***p <0.001, Student's t-test). (H) Histogram
862 showing mRNA expression levels of innate immune response genes of the AMP
863 family (*Attc*, *DiptB* and *Mtk*) in the adult brain. Expression was increased in all cases
864 following treatment. The *RPL28* gene served as an internal reference. Results are
865 means ± SEM (***p <0.001, Student's t-test). (I, J) The number of Dcp-1^+ puncta
866 (green) increased in injured adult brains 24 h after TBI. Scale bar = 50 μm. (K)
867 Quantification of Dcp-1^+ puncta. Error bars denote SEM (**p <0.01, Student's t-tests).
868 Results are means ± SEM. (L–M") Apoptotic debris labelled with anti-Dcp-1
869 antibodies. Glial and neuronal nuclei are labelled with anti-Repo (L) and anti-Elav (M)
870 antibodies, respectively. Three representative images (L–L" and M–M") for each pair
871 of antibody staining are shown. Scale bar = 20 μm.

872

873 **Figure 2. TBI alters glial morphology and upregulates Mmp1 expression.**

874 (A–C) Representative images of astrocyte membranes labelled with *mCD8::GFP*
875 driven by the astrocyte driver *R86E01-Gal4*. Co-expression of *UAS-Redstinger* labels
876 astrocyte nuclei. GFP intensities are increased at 4 h (B) and 24 h (C) after injury. The
877 rectangle defined by white dash lines denotes antennal lobes. Scale bars = 100 μm. (D)

878 Quantification of GFP intensity at different timepoints after TBI. Results are
879 means ± SEM (**p <0.01, Student's t-test). (E, F) MARCM analysis reveals single
880 astrocytes with evenly distributed GFP^+ cellular processes without injury (E) and an
881 increased number of GFP^+ puncta at 24 h after injury (F). Arrows denote GFP^+
882 accumulations in astrocyte processes. White dots demarcate neuropils. Anti-Repo
883 antibodies labelled glial nuclei. TO-PRO labelled all nuclei. Insets show the
884 morphology of a glial soma before and after injury. Scale bar = 10 μm. (G)
885 Quantification of GFP^+ puncta in astrocyte processes before and after injury. (H)
886 Quantification of the astrocyte soma diameter surrounding ALs after injury. Results
887 are means ± SEM (***p <0.001, Student's t-test). (I–J", M–N") Representative images
888 of ALs co-labelled with GFP and Mmp1 (magenta) in uninjured and injured adult
889 brains. (J–J") GFP-labelled astrocyte membranes (green) overlapped with Mmp1
890 (magenta) after injury. (N–N") After injury, Mmp1 co-localizes with GFP-labelled
891 ENG (*R56F03-Gal4*) membranes (green). Arrows show Mmp1-GFP colocalization in
892 L" and P". Scale bar = 20 μm. (K, L) Graph showing fluorescence intensity per pixel
893 in each channel for the inset in I" and J" of the astrocyte membrane and Mmp1 along a
894 line drawn through a cell body. (O, P) Graph showing fluorescence intensity per pixel
895 in each channel for the inset in M" and N" of the ENG membrane and Mmp1 along a
896 line drawn through the process of ENG. (Q) Quantification of Mmp1 intensity in I–J"
897 and M–N". Ast is the short of astrocytes. Results are means ± SEM (**p <0.01,
898 Student's t-test).
899
900 **Figure 3. Transcriptome analysis of astrocytes reveals upregulation of**
901 **injury-related and innate immunity genes.**
902 (A) After dissection, *Drosophila* brains were disrupted and the cell suspension was
903 subjected to FACS. Astrocyte cDNAs were amplified by the Smart-seq2 method and a
904 cDNA library was constructed. A subset of upregulated genes from RNA-seq
905 screening was validated by quantitative real-time PCR. (B, C) Volcano plots of the

906 gene expression analysis; 522 differentially expressed genes (416 upregulated, 106
907 downregulated) in astrocytes were detected at 4 h after injury (B), and 357
908 differentially expressed genes (229 upregulated, 129 downregulated) in astrocytes
909 were detected at 24 h after injury (C). The threshold for differential expression was set
910 at $\log_2$FC = 1 with an adj. p <0.01. FC = fold change; adj. = adjusted (for multiple
911 comparisons by the Benjamin-Hochberg procedure). (D) Heatmap of the expression
912 of a small set of representative genes, including *draper*, *Jra* and *kay*, previously
913 identified as essential factors during glial clearance of severed axons. (E) Quantitative
914 real-time PCR validation of a subset of upregulated genes from RNA-seq screening.
915 Error bars represent SEM. Results are means ± SEM (*p <0.05, **p <0.01 and
916 ***p <0.001 by Student's t tests).
917
918 **Table 1. Upregulated genes related to receptors and endocytosis.**
919
920 **Figure 4. Pvr, Jra and kay are required for Mmp1 upregulation after TBI.**
921 (A–F) Knockdown of Pvr, Jra or kay by *R86E01-Gal4* driven RNAi in astrocytes
922 suppresses Mmp1 upregulation after TBI. Scale bar = 100 μm. All images are
923 projections of 25–30 μm immunostaining slices (one image per 1 μm slice). Arrows
924 show Mmp1 signals. (F) Quantification of Mmp1 intensity in different genotypes.
925 Results are means ± SEM (*p <0.05 by Student's t-test).
926
927 **Figure 5. Pvr is required for AP-1 upregulation after TBI.**
928 (A–B") Adult brains showing increased *TRE-dsRed* (an AP-1 reporter) expression at
929 24 h after TBI. (C–D") Overexpression of Pvr in astrocytes leads to upregulated
930 dsREd expression compared with control flies. Scale bar = 100 μm. (E–F")
931 Knockdown of Pvr in astrocytes causes downregulation of dsRed expression
932 compared with control flies after TBI. (G–H") Overexpression of Pvr and knockdown
933 of Jra at the same time in astrocytes causes downregulation of dsRed and Mmp1 after

934 TBI compared with controls. (I–J") Overexpression of Pvr and knockdown of kay in
935 astrocytes at the same time causes downregulation of dsRed and Mmp1 after TBI
936 compared with controls. (K, L) Quantification of Mmp1 (K) and dsRed (L) intensity.
937 Results are means ± SEM **p <0.01, ***p <0.001, Student's t-tests.
938
939 **Figure 6. Inhibition of dynamin activity increases the expression levels of Pvr**
940 **and dsRed after TBI.**
941 (A, B) Representative Pvr immunostaining (green), dsRed (magenta) and β-gal
942 intensity (gray) in control animals (*TRE-dsRed;R86E01-Gal4>UAS-nLacZ*) at 4 h
943 after TBI. All images are projections of 25–30 μm immunostaining slices (one image
944 per 1 μm slice). (C, D) Representative Pvr immunostaining (green), dsRed (magenta)
945 and Mmp1 intensity (gray) in shi^{ts}-expressing animals
946 (*TRE-dsRed;R86E01-Gal4>UAS-*shi^{ts}) at 4 h after TBI. For thermogenetic
947 inactivation of dynamin, flies after TBI were incubated at intermittent temperature at
948 32°C (32°C for 30 min, and then back to 23°C for 30 min, for four rounds, four hours
949 in total) until dissection. (E, F) Quantification of Pvr and dsRed intensity in different
950 genotypes. Results are means ± SEM (*p <0.05).
951
952 **Figure 7. Knockdown of endocytic trafficking-related genes up-regulates**
953 **expression of AP-1 and Mmp1upon TBI**
954 (A, H) Representative Mmp1 immunostaining (magenta) and dsRed intensity
955 (magenta) in control animals (*R86E01-Gal4*) at 24 h after TBI. (B–D, I–K)
956 Knockdown of *Arpc2*, *cpa*, and *cpb* in astrocytes results in further upregulation of
957 Mmp1 and dsRed upon TBI. All images are projections of 25–30 μm immunostaining
958 slices (one image per 1 μm slice). (E–G, L–N) Knockdown of *Stam*, *Chmp1* or *Vps24*,
959 components of ESCRT, in astrocytes had no influence on Mmp1 and dsRed
960 upregulation compared with control after TBI (A, H). All images are projections of
961 25–30 μm immunostaining slices (one image per 1 μm slice). (O, P) Quantification of

962 Mmp1 and dsRed intensity in different genotypes. Results are means ± SEM
963 (*p <0.05, **p <0.01, ***p <0.001, Student's t-tests). (Q) Schematic diagram of Pvr–
964 AP-1–MMP1 signaling activated by TBI in astrocytes. AP-1 transcription factor
965 complex is composed of Jra and kay.
966

967 **Figure S1. No cell proliferation is detected in adult brains.**

968 (A–C") Drosophila brains expressing the S-phase activity reporter PCNA::GFP at
969 larval and adult stages were dissected and co-stained with the mitotic marker
970 phosphohistone H3 (pH3). As controls, uninjured larval brains exhibit both GFP^+ and
971 $pH3^+$ signals, indicating that cells are proliferative at this stage (A–A"). In both
972 uninjured and injured adult brains, no apparent GFP^+ and $pH3^+$ signals were detected
973 (B–C"). Scale bar = 50 μm. (D–F) No $pH3^+$ cells were observed in adult brains at
974 different time points of 48 h (D), 72 h (E) and 5 days (F) after TBI. Scale bar = 50
975 μm.

976

977 **Figure S2. Sorting of adult astrocytes by FACS.**

978 (A) To discriminate between healthy and damaged or dying cells, side scatter (SSC-A,
979 log) and forward scatter (FSC-A, log) were plotted. Higher SSC-A signals indicate
980 increased granularity and therefore likely dying cells. Thus, one should define the
981 sorting gate as the population with the lower SSC-A signal (P1). (P2) Exclude cell
982 clusters by sorting only events with a low FSC width (FSC-W) versus similar area
983 (FSC-A) signal to get exact single cell. (P3) To gate for RFP^+ cells, plotted the signal
984 from the excitation of cells with the 568-nm laser (PE-Texas Red-A, log) against the
985 signal from the SSC-A. The population with the higher PE-Texas Red-A signal was
986 the candidate cells cluster. The strategy for FACS is shown at the lower right corner.
987 (B–C') A population of cells with strong RFP signal was purified from adult flies of
988 *R86E01-Gal4>UAS-Redstinger*. (B and B') Confocal images of representative
989 astrocytes before and after sorting by FACS. Scale bar = 50 μm. (C and C') As
990 cell-permeant MitoTracker labels mitochondria of live cells, cells after FACS both
991 labelled by RFP and MitoTracker. Scale bar = 10 μm. (D) A Principal Component
992 Analysis of all biological replicates (uninjured versus injured) revealing genes
993 expressed at absolute value of logarithmic fold change (log_2FC) > 1.0.

994 **Figure S3. GO analysis of differentially expressed genes at 4 h and 24 h after**
995 **injury.**
996 Scatterplot showing GO functional enrichment results for differentially expressed
997 genes of astrocytes in the brain at 4 h (A) and 24 h (B) after injury, $p < 0.01$.
998
999 **Figure S4. Overexpression of Jra or kay does not enhance the expression of**
1000 **TRE-RFP and Mmp1 in adult brain after TBI.**
1001 (A, B") Fly brains showing TRE-RFP expression before and 24 h after TBI. (C–F")
1002 overexpression of Jra or kay in astrocytes shows no apparent changes of RFP and
1003 Mmp1 staining signals compared with control flies with or without brain injury
1004 (*TRE-dsRed/UAS-Jra* or *kay*; *R86E01-Gal4/+*). Scale bar = 100 μm. (G, H)
1005 Knockdown of AdoR in astrocytes inhibits the expression of Mmp1 after TBI.
1006 However, Knockdown of AdoR in astrocytes does not inhibit the expression of dsRed.
1007 (I, J) Quantification of Mmp1 and dsRed intensity before and after injury in different
1008 genotypes. Data are present as means ± SEM; $*p < 0.05$, $**p < 0.01$, $***p < 0.001$ by
1009 Student's *t* tests.
1010
1011 **Figure S5. Pvr is upregulated in astrocytes in the adult brains after TBI.**
1012 Immunostainings of Pvr in the control brains showed Pvr was expressed at low levels
1013 in uninjured brains (A) and its expression was upregulated at 24 h after TBI (B). (C, D)
1014 Knockdown of Pvr in astrocytes reduced Pvr expression upon TBI. (E, F) Pvr
1015 overexpression in astrocytes increased Pvr expression upon TBI. Scale bar = 100 μm.
1016 (G) Quantification of Pvr intensity in A–E. Data are present as means ± SEM;
1017 $*p < 0.05$, $***p < 0.001$ by Student's *t* tests.
1018
1019 **Figure S6. Astrocytes do not engulf debris in adult brain after TBI.**
1020 (A–C ") Confocal images are single z-confocal slices. Astrocytes membranes were
1021 labeled with GFP (*UAS-mCD8::GFP* expression driven by *R86E01-Gal4*; green);

1022 nuclei were labeled with TO-PRO3 (blue), while axons were labeled with Ncad (a cell
1023 adhesion molecule; magenta). Inset, high-magnification view of the boxed region.
1024 Scale bars = 10 μm. (D–F) The graph shows fluorescence intensity in each channel for
1025 the inset in A–C, respectively, of GFP, Ncad and nuclear staining along a line drawn
1026 through an astrocyte nucleus.

Figure 1

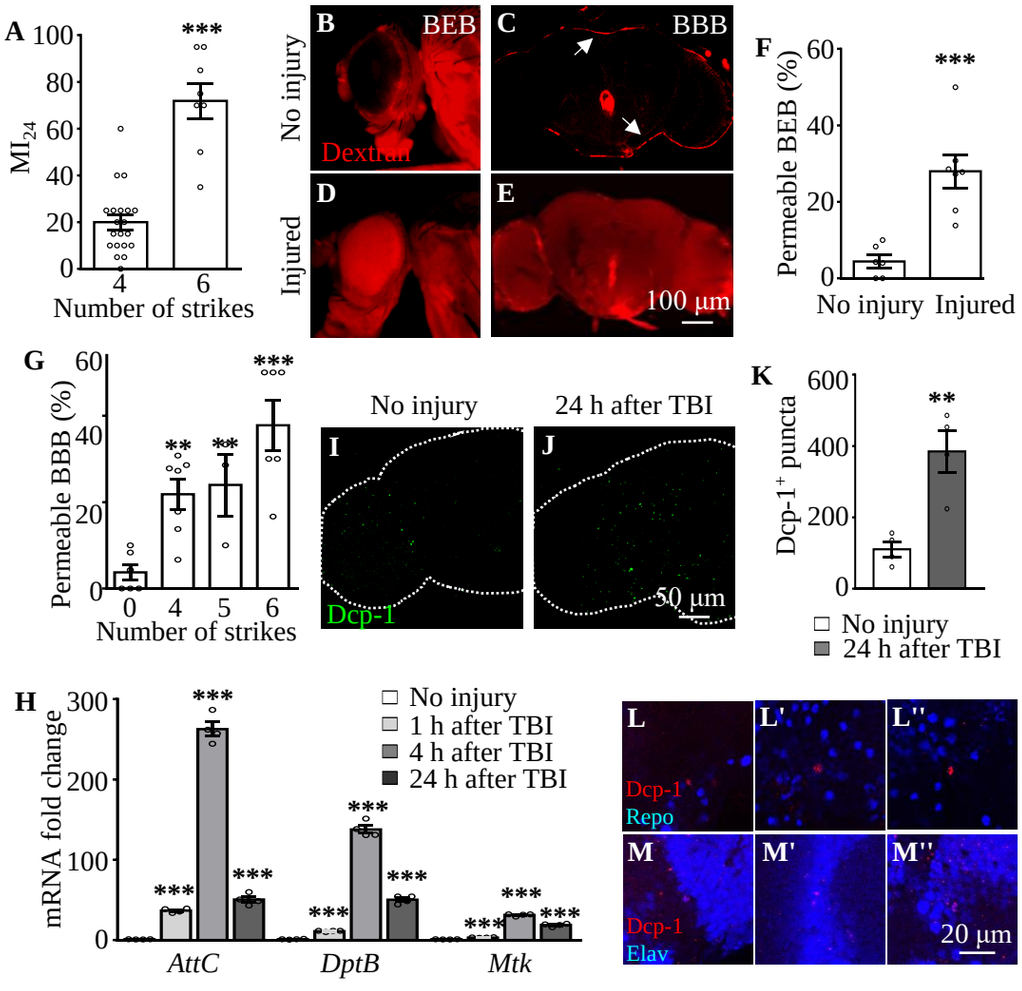
A
ML_{24}
Number of strikes
B BEB
C BBB
No injury
Injured
Dextran
D
E
100 µm
F
Permeable BEB (%)
No injury
Injured
G
Permeable BBB (%)
Number of strikes
No injury
24 h after TBI
I
J
Dcp-1
50 µm
K
Dcp-1+ puncta
No injury
24 h after TBI
H
mRNA fold change
No injury
1 h after TBI
4 h after TBI
24 h after TBI
AttC
DptB
Mtk
L
L'
L''
Dcp-1
Repo
M
M'
M''
Dcp-1
Elav
20 µm

Figure 2

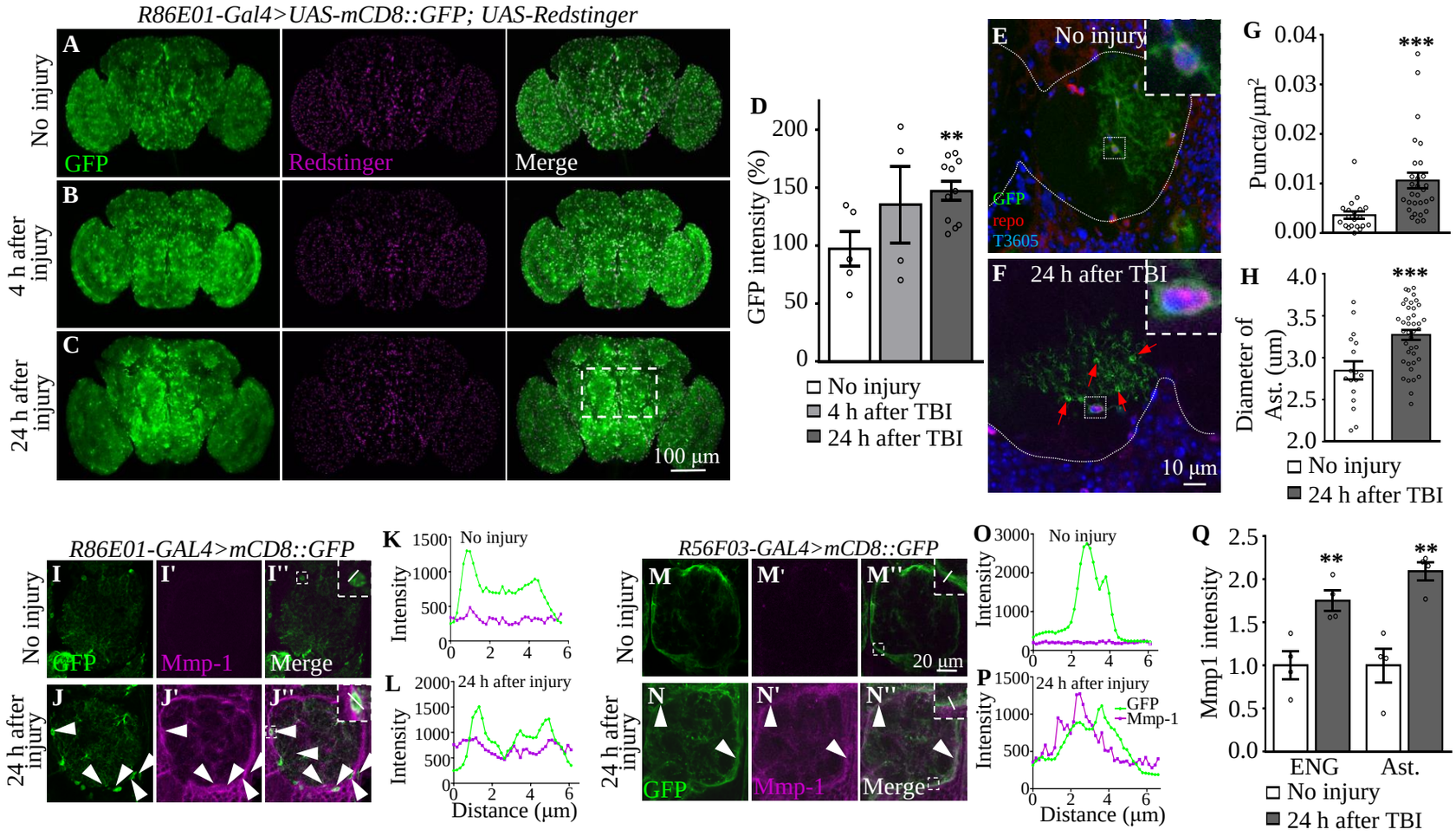
R86E01-Gal4>UAS-mCD8::GFP; UAS-Redstinger
A
B
C
No injury
4 h after injury
24 h after injury
GFP
Redstinger
Merge
100 µm
D
GFP intensity (%)
No injury
4 h after TBI
24 h after TBI
E
No injury
GFP
repo
T3605
F
24 h after TBI
10 µm
G
Puncta/µm²
H
Diameter of Ast. (um)
R86E01-GAL4>mCD8::GFP
I
I'
I''
J
J'
J''
Mmp-1
K
L
Intensity
Distance (µm)
R56F03-GAL4>mCD8::GFP
M
M'
M''
N
N'
N''
20 µm
O
P
GFP
Mmp-1
Q
Mmp1 intensity
ENG
Ast.

Figure 3

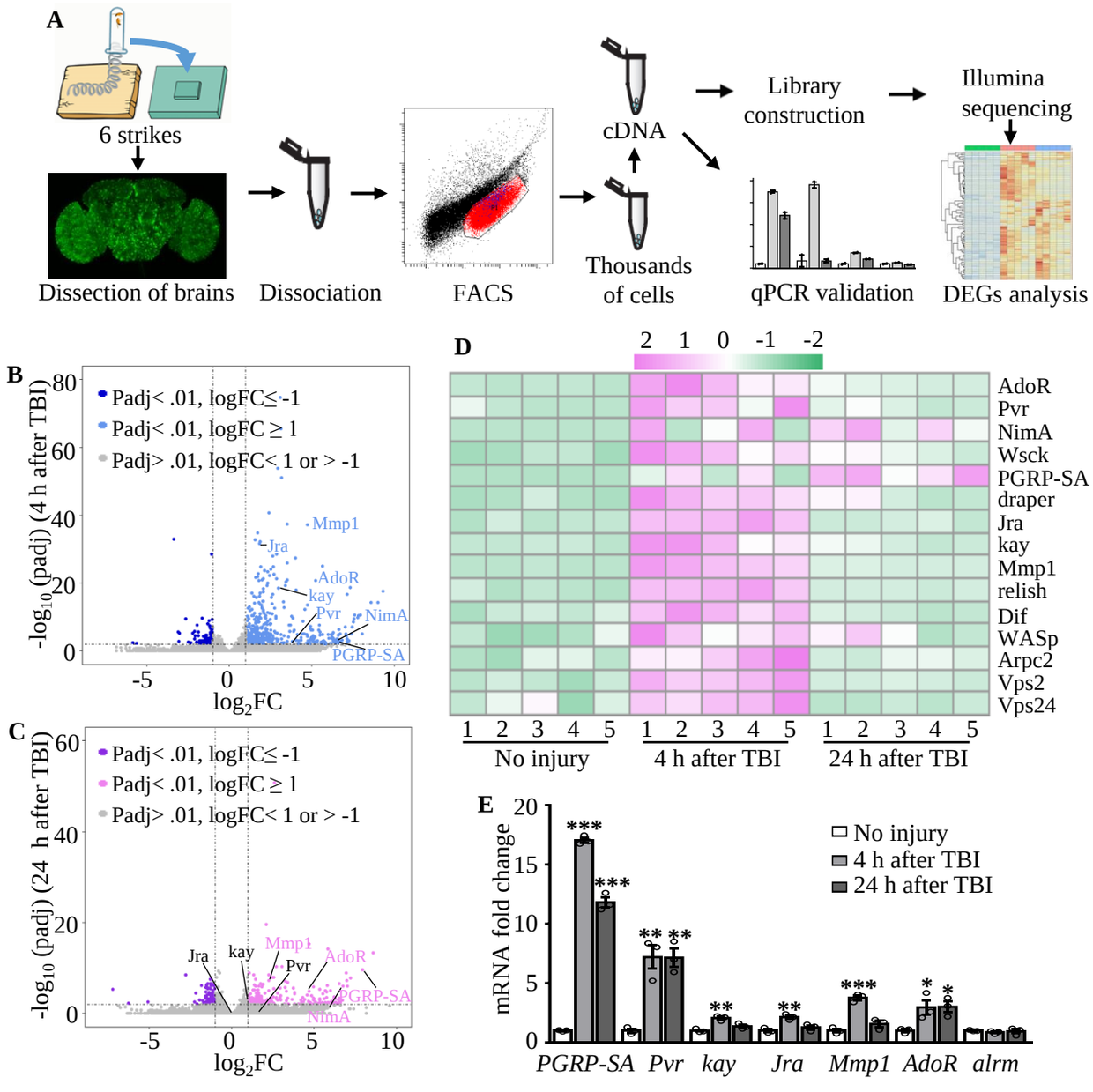
A
6 strikes
Dissection of brains
Dissociation
FACS
Thousands of cells
cDNA
Library construction
Illumina sequencing
qPCR validation
DEGs analysis
B
Padj< .01, logFC≤ -1
Padj< .01, logFC ≥ 1
Padj> .01, logFC< 1 or > -1
-log10 (padj) (4 h after TBI)
log2FC
Mmp1
Jra
AdoR
kay
Pvr
NimA
PGRP-SA
C
Padj< .01, logFC≤ -1
Padj< .01, logFC ≥ 1
Padj> .01, logFC< 1 or > -1
-log10 (padj) (24 h after TBI)
log2FC
Jra
kay
Mmp1
Pvr
AdoR
PGRP-SA
NimA
D
2 1 0 -1 -2
AdoR
Pvr
NimA
Wsck
PGRP-SA
draper
Jra
kay
Mmp1
relish
Dif
WASp
Arpc2
Vps2
Vps24
No injury
4 h after TBI
24 h after TBI
E
mRNA fold change
No injury
4 h after TBI
24 h after TBI
PGRP-SA
Pvr
kay
Jra
Mmp1
AdoR
alrm

Table 1

Genes in *Drosophila*	Conserved genes in mouse	Conserved genes in human	4 h after injury (FC)	24 h after injury (FC)
Pvr	pdgfr/vegfr	VEGFR	13.83	2.79
AdoR	Adora2a	ADORA2B	37.53	7.73
Mmp1	Mmp14	MMP14	26.35	4.79
Jra	Jun	JUN	3.58	1.18
kay	FOSL2	FOS	6.23	1.77
cpa	Capza2	CAPZA1	3.43	1.72
cpb	Capzb	CAPZB	2.01	1.25
Stam	Stam2	STAM	2.14	1.46
Chmp1	Chmp1b	CHMP1B	2.16	0.92
Vps24	Chmp3	CHMP3	2.11	0.87

Figure 4

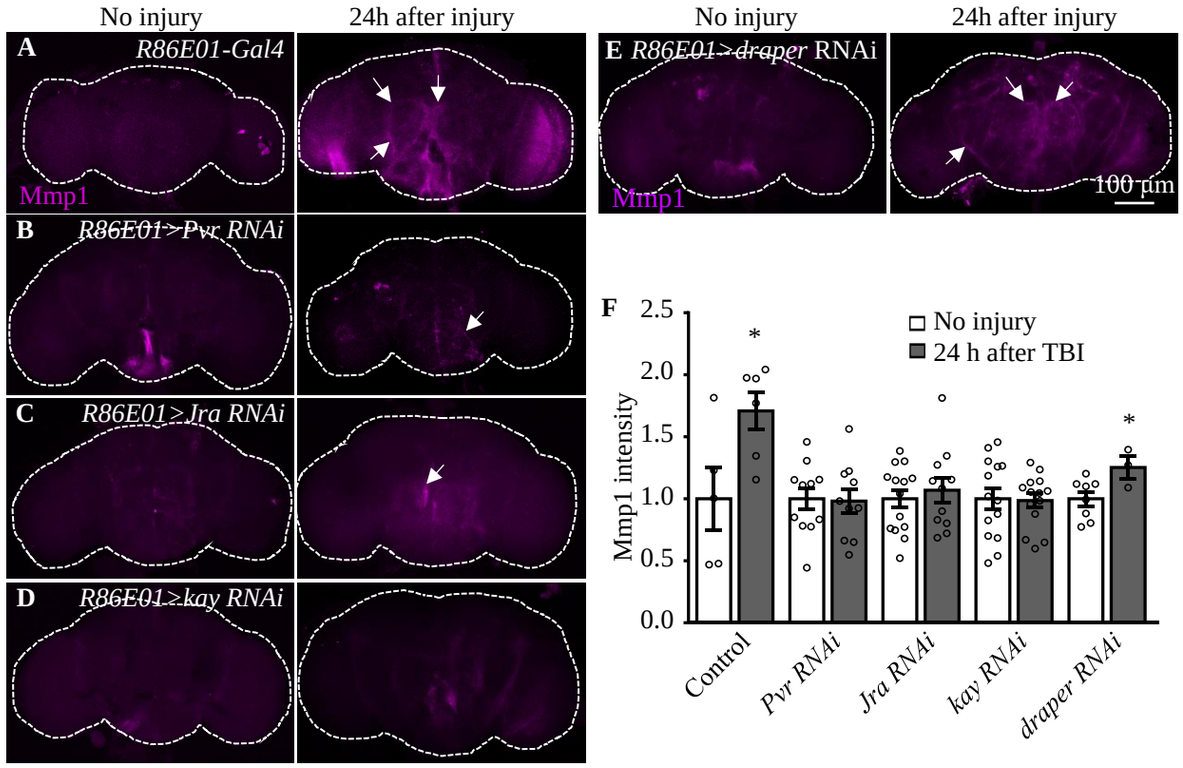
No injury
24h after injury
A
R86E01-Gal4
Mmp1
B
R86E01>Pvr RNAi
C
R86E01>Jra RNAi
D
R86E01>kay RNAi
No injury
24h after injury
E
R86E01>draper RNAi
Mmp1
100 µm
F
No injury
24 h after TBI
Mmp1 intensity
2.5
2.0
1.5
1.0
0.5
0.0
*
*
Control
Pvr RNAi
Jra RNAi
kay RNAi
draper RNAi

Figure 5

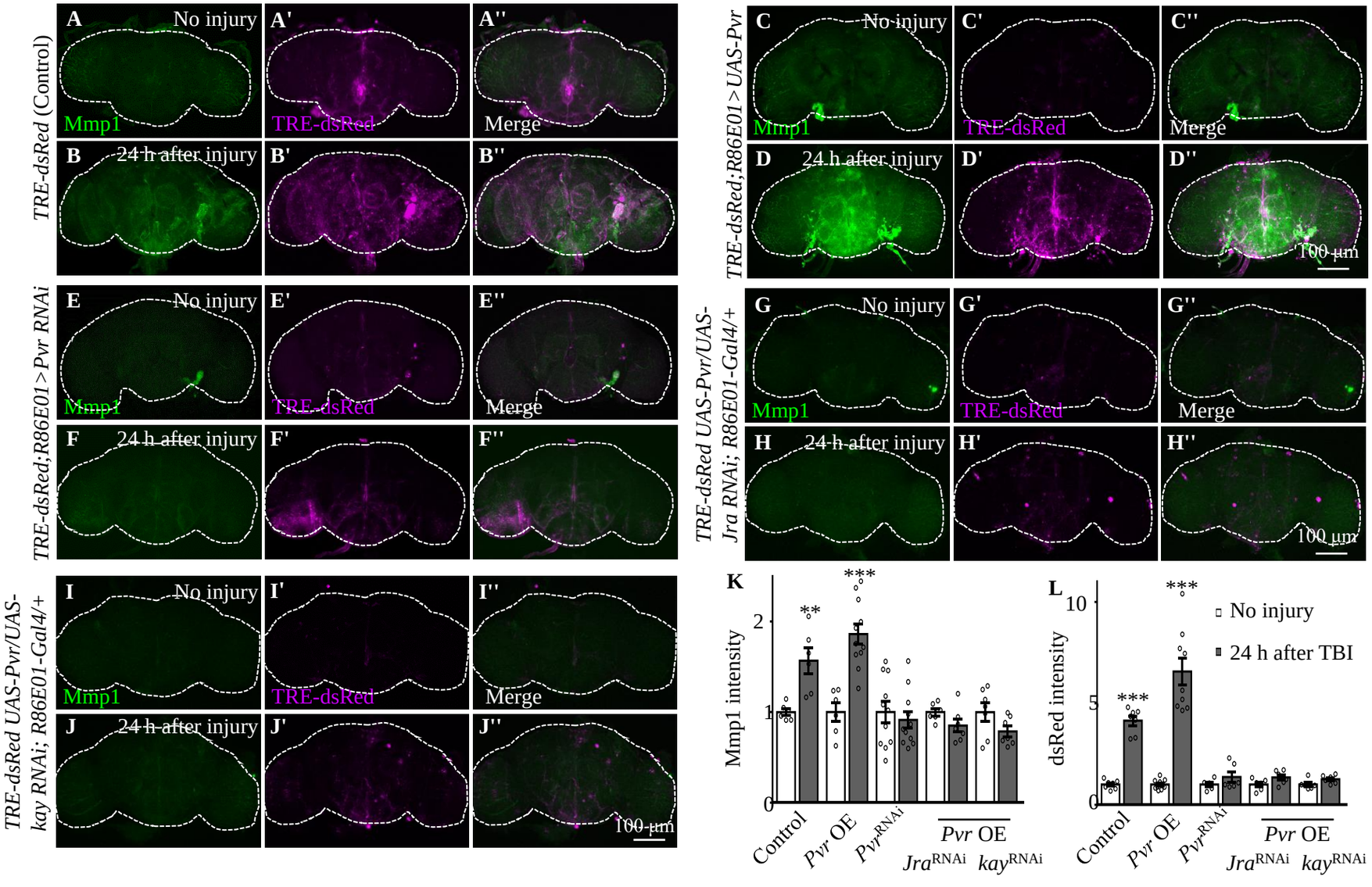
TRE-dsRed (Control)
TRE-dsRed;R86E01>Pvr RNAi
TRE-dsRed UAS-Pvr/UAS-kay RNAi; R86E01-Gal4/+
TRE-dsRed;R86E01>UAS-Pvr
TRE-dsRed UAS-Pvr/UAS-Jra RNAi; R86E01-Gal4/+
A No injury
A'
A''
B 24 h after injury
B'
B''
C No injury
C'
C''
D 24 h after injury
D'
D''
E No injury
E'
E''
F 24 h after injury
F'
F''
G No injury
G'
G''
H 24 h after injury
H'
H''
I No injury
I'
I''
J 24 h after injury
J'
J''
Mmp1
TRE-dsRed
Merge
100 µm
K
Mmp1 intensity
No injury
24 h after TBI
Control
Pvr OE
Pvr^RNAi
Pvr OE
Jra^RNAi
kay^RNAi
L
dsRed intensity

Figure 6

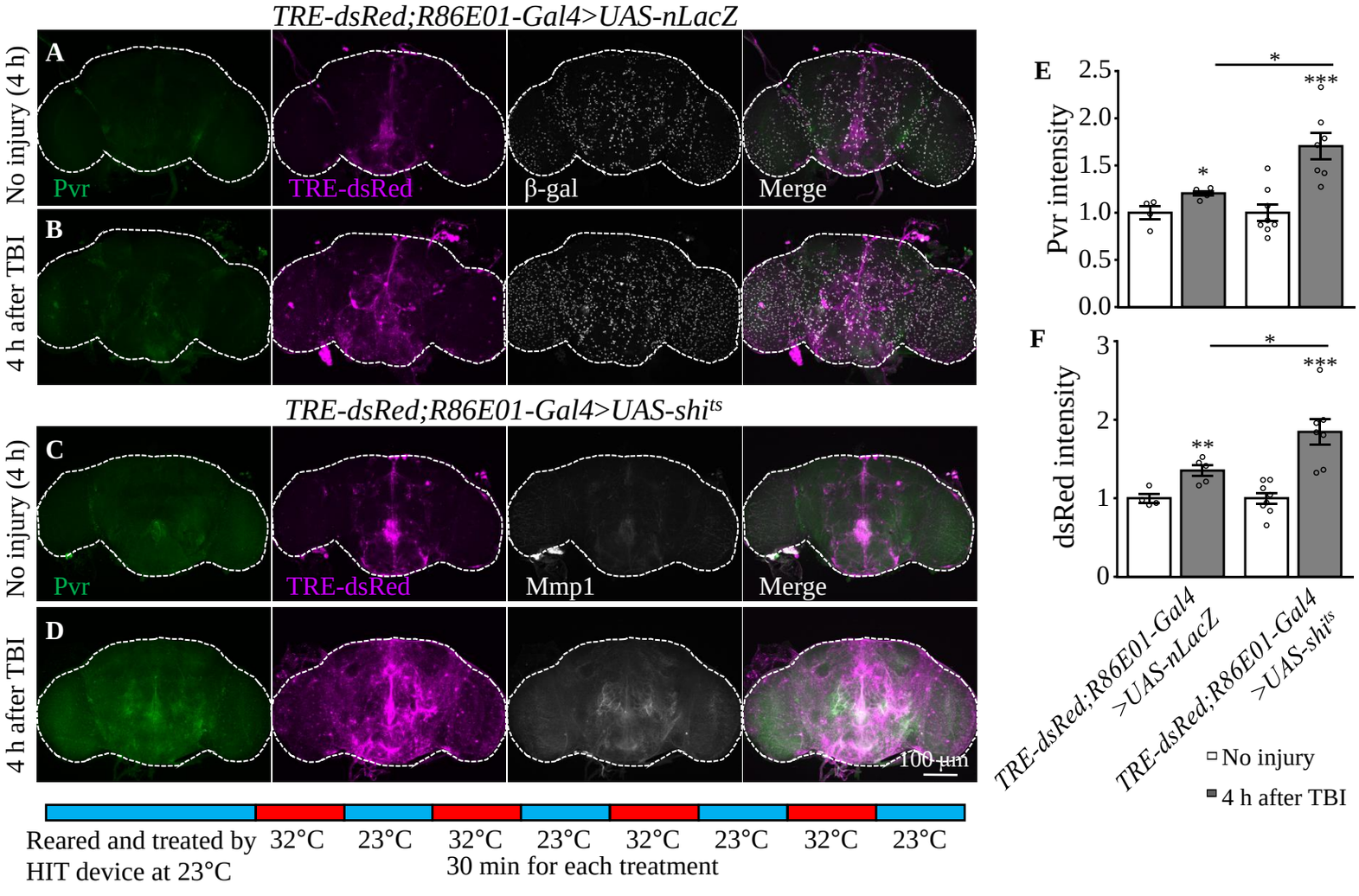
TRE-dsRed;R86E01-Gal4>UAS-nLacZ
A
No injury (4 h)
Pvr
TRE-dsRed
β-gal
Merge
B
4 h after TBI
TRE-dsRed;R86E01-Gal4>UAS-shi^ts
C
No injury (4 h)
Pvr
TRE-dsRed
Mmp1
Merge
D
4 h after TBI
100 μm
Reared and treated by HIT device at 23°C
32°C
23°C
32°C
23°C
32°C
23°C
32°C
23°C
30 min for each treatment
E
Pvr intensity
2.5
2.0
1.5
1.0
0.5
0.0
*
***
*
F
dsRed intensity
3
2
1
0
*
***
**
TRE-dsRed;R86E01-Gal4 >UAS-nLacZ
TRE-dsRed;R86E01-Gal4 >UAS-shi^ts
No injury
4 h after TBI

Figure 7

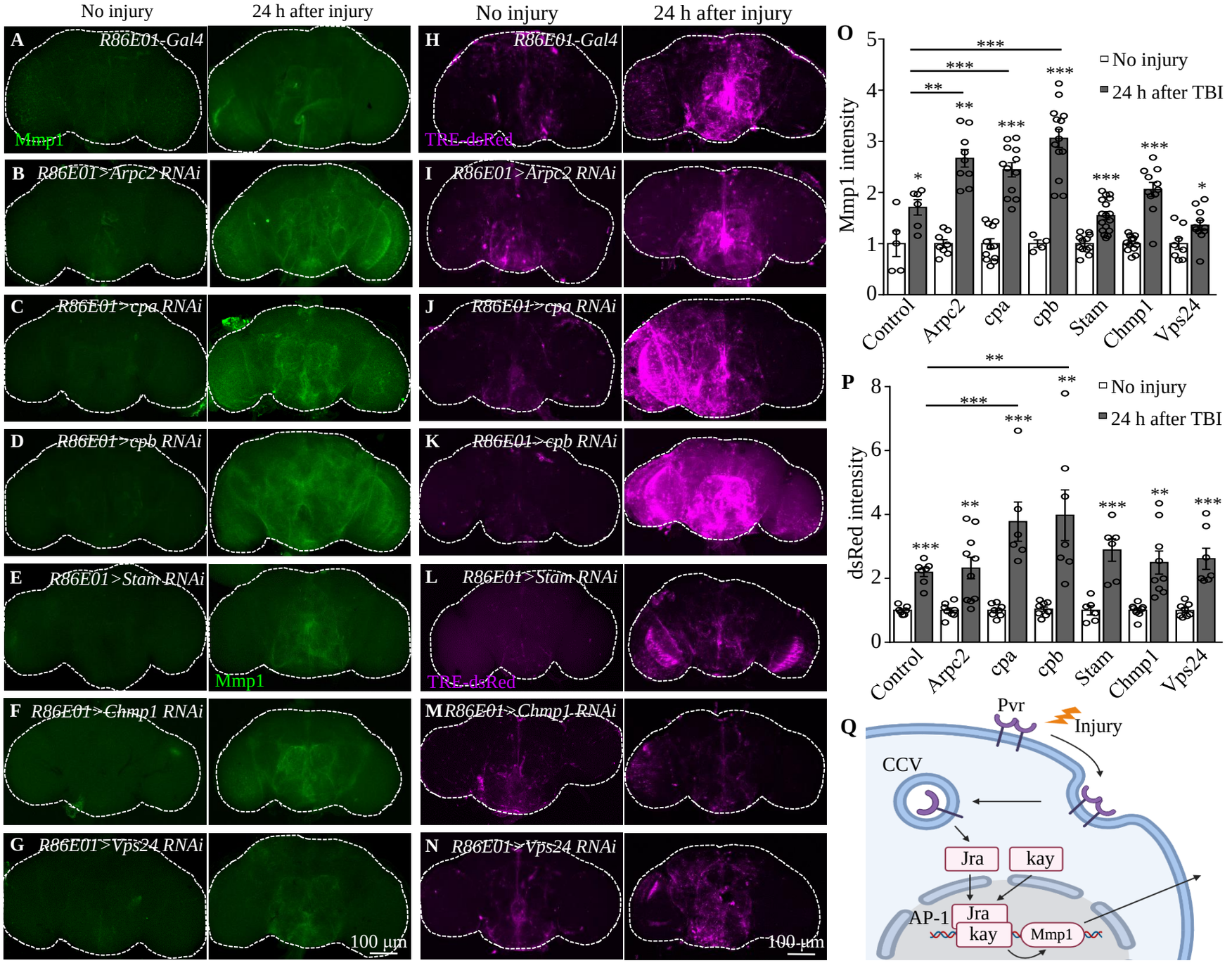
No injury
24 h after injury
No injury
24 h after injury
A R86E01-Gal4
Mmp1
H R86E01-Gal4
TRE-dsRed
B R86E01>Arpc2 RNAi
I R86E01>Arpc2 RNAi
C R86E01>cpa RNAi
J R86E01>cpa RNAi
D R86E01>cpb RNAi
K R86E01>cpb RNAi
E R86E01>Stam RNAi
Mmp1
L R86E01>Stam RNAi
TRE-dsRed
F R86E01>Chmp1 RNAi
M R86E01>Chmp1 RNAi
G R86E01>Vps24 RNAi
100 μm
N R86E01>Vps24 RNAi
100 μm
O
Mmp1 intensity
No injury
24 h after TBI
Control
Arpc2
cpa
cpb
Stam
Chmp1
Vps24
P
dsRed intensity
No injury
24 h after TBI
Control
Arpc2
cpa
cpb
Stam
Chmp1
Vps24
Q
Pvr
Injury
CCV
Jra
kay
AP-1
Jra
kay
Mmp1

Figure S1

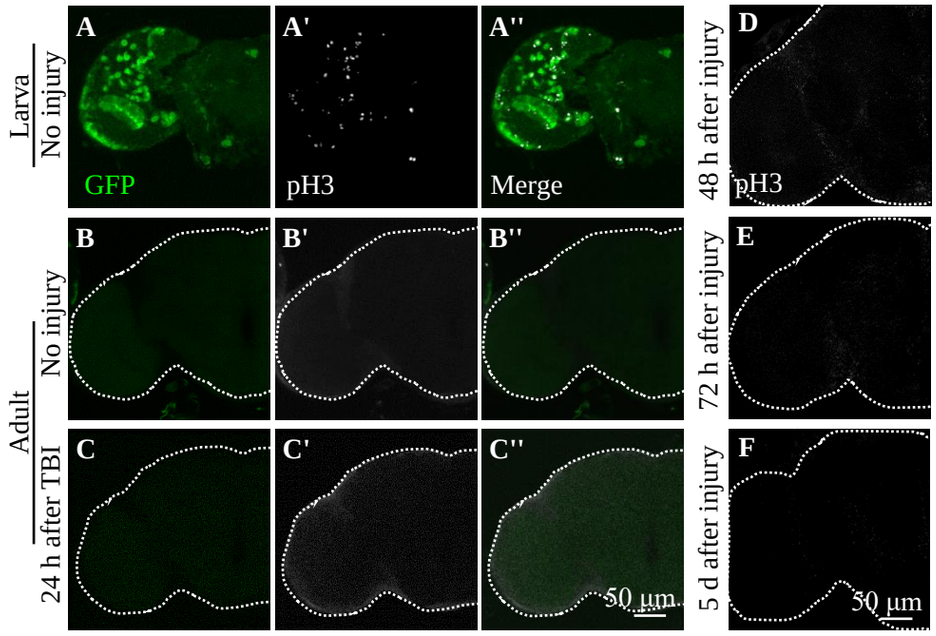
Larva
No injury
Adult
No injury
24 h after TBI
A
A'
A''
GFP
pH3
Merge
B
B'
B''
C
C'
C''
50 µm
48 h after injury
72 h after injury
5 d after injury
D
E
F
pH3
50 µm

Figure S2

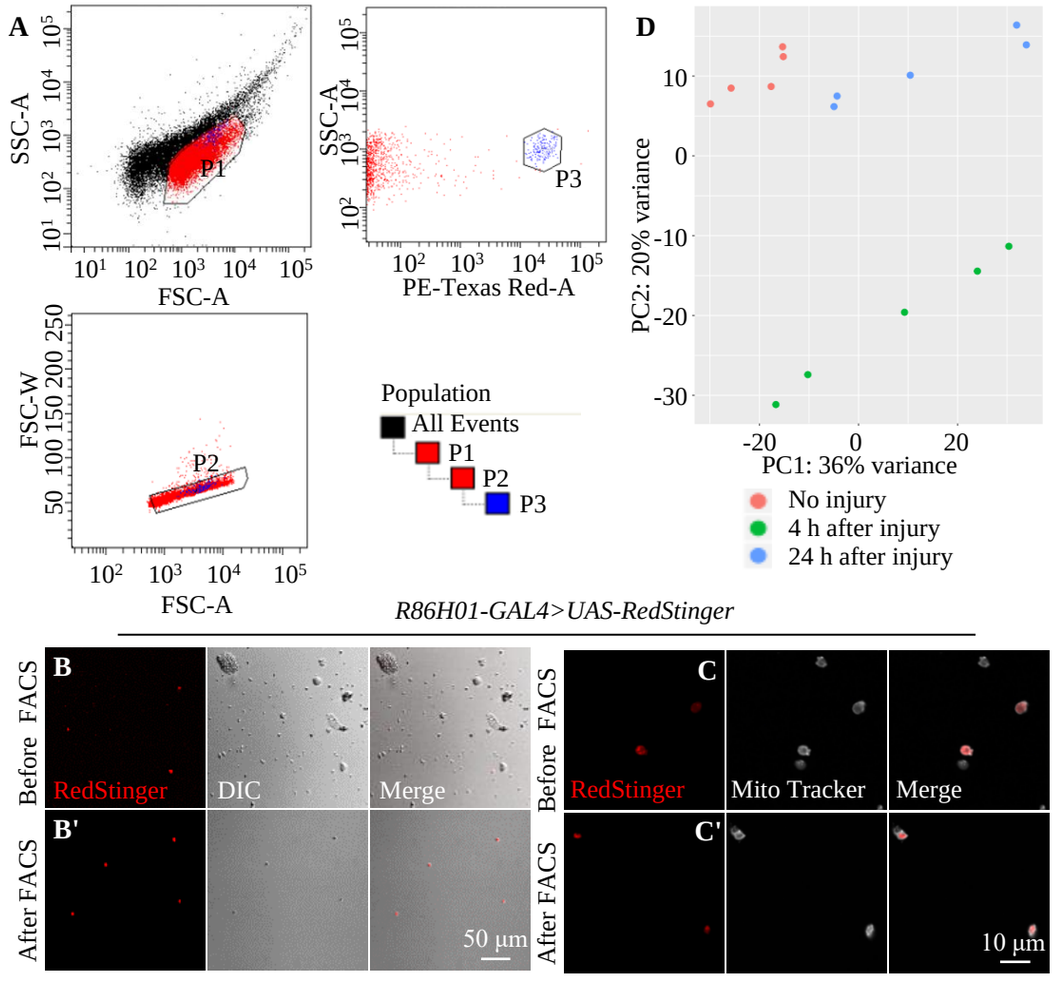
A
SSC-A
FSC-A
P1
SSC-A
PE-Texas Red-A
P3
FSC-W
FSC-A
P2
Population
All Events
P1
P2
P3
D
PC2: 20% variance
PC1: 36% variance
No injury
4 h after injury
24 h after injury
R86H01-GAL4>UAS-RedStinger
Before FACS
After FACS
B
RedStinger
DIC
Merge
B'
50 µm
C
RedStinger
Mito Tracker
Merge
C'
10 µm

Figure S3

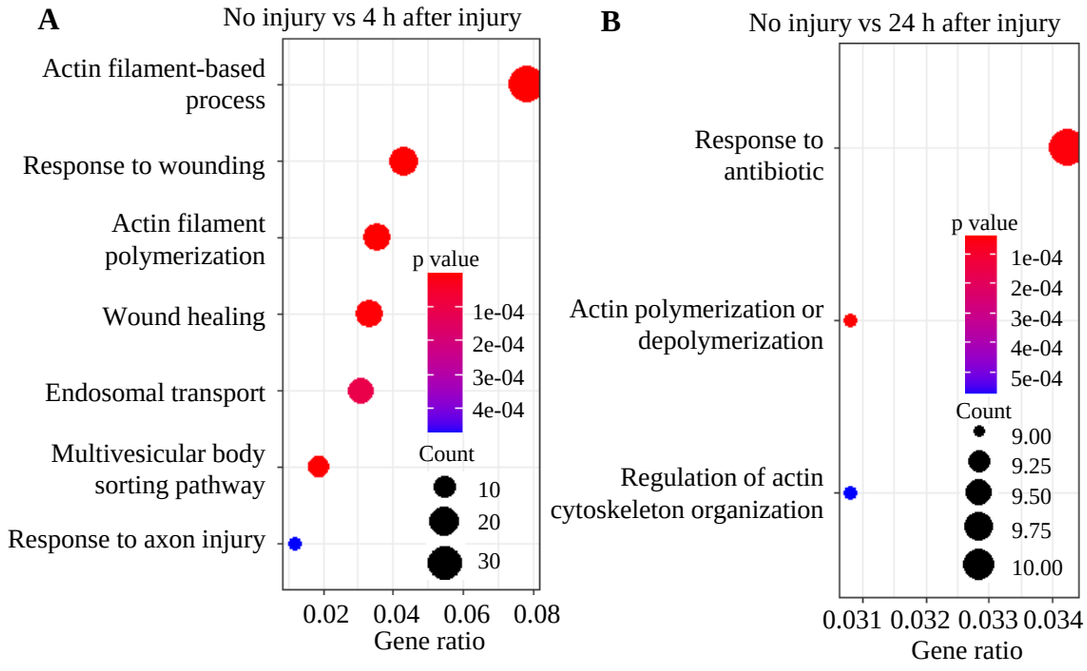
A
No injury vs 4 h after injury
Actin filament-based process
Response to wounding
Actin filament polymerization
Wound healing
Endosomal transport
Multivesicular body sorting pathway
Response to axon injury
p value
1e-04
2e-04
3e-04
4e-04
Count
10
20
30
0.02
0.04
0.06
0.08
Gene ratio
B
No injury vs 24 h after injury
Response to antibiotic
Actin polymerization or depolymerization
Regulation of actin cytoskeleton organization
p value
1e-04
2e-04
3e-04
4e-04
5e-04
Count
9.00
9.25
9.50
9.75
10.00
0.031
0.032
0.033
0.034
Gene ratio

Figure S4

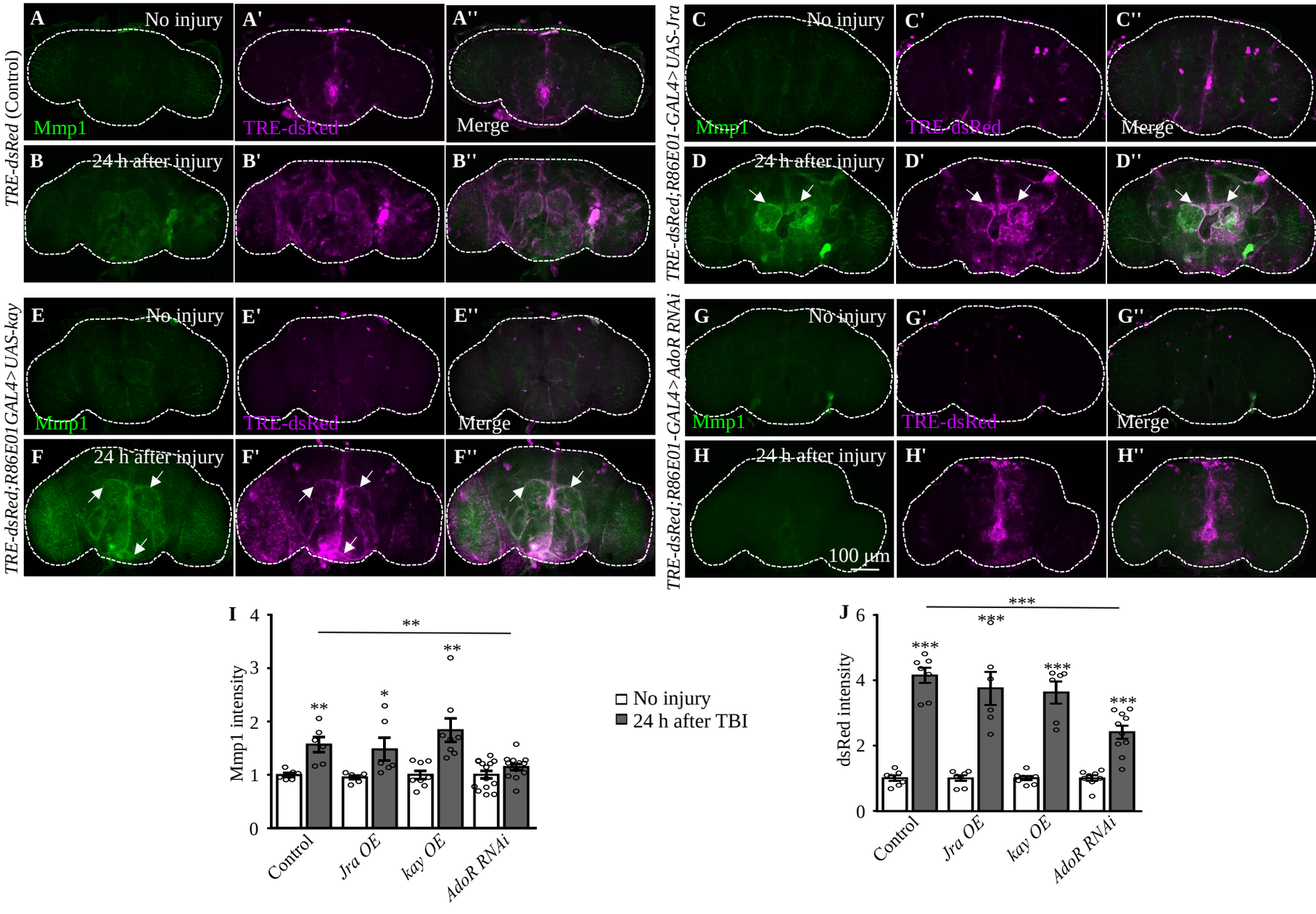
TRE-dsRed (Control)
TRE-dsRed;R86E01-GAL4>UAS-Jra
TRE-dsRed;R86E01-GAL4>UAS-kay
TRE-dsRed;R86E01-GAL4>AdoR RNAi
A No injury
A'
A''
Mmp1
TRE-dsRed
Merge
B 24 h after injury
B'
B''
C No injury
C'
C''
D 24 h after injury
D'
D''
E No injury
E'
E''
F 24 h after injury
F'
F''
G No injury
G'
G''
H 24 h after injury
H'
H''
100 μm
I
Mmp1 intensity
No injury
24 h after TBI
Control
Jra OE
kay OE
AdoR RNAi
J
dsRed intensity

Figure S5

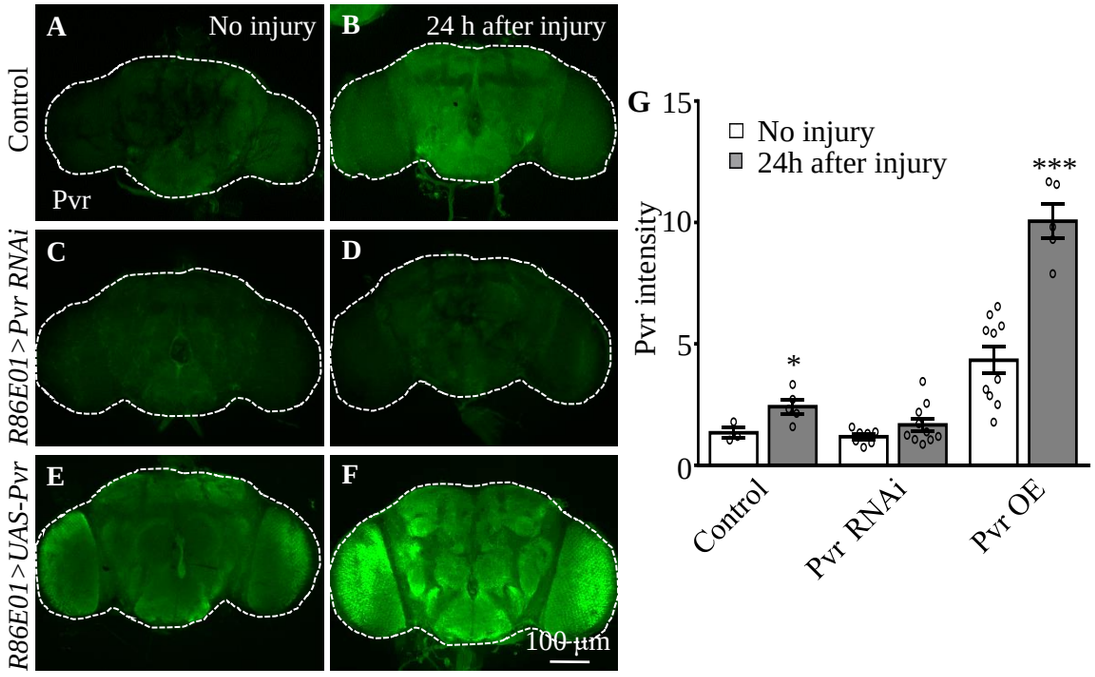
A
No injury
B
24 h after injury
Control
Pvr
C
D
R86E01>Pvr RNAi
E
F
R86E01>UAS-Pvr
100 µm
G
No injury
24h after injury
Pvr intensity
15
10
5
0
*
***
Control
Pvr RNAi
Pvr OE

Figure S6

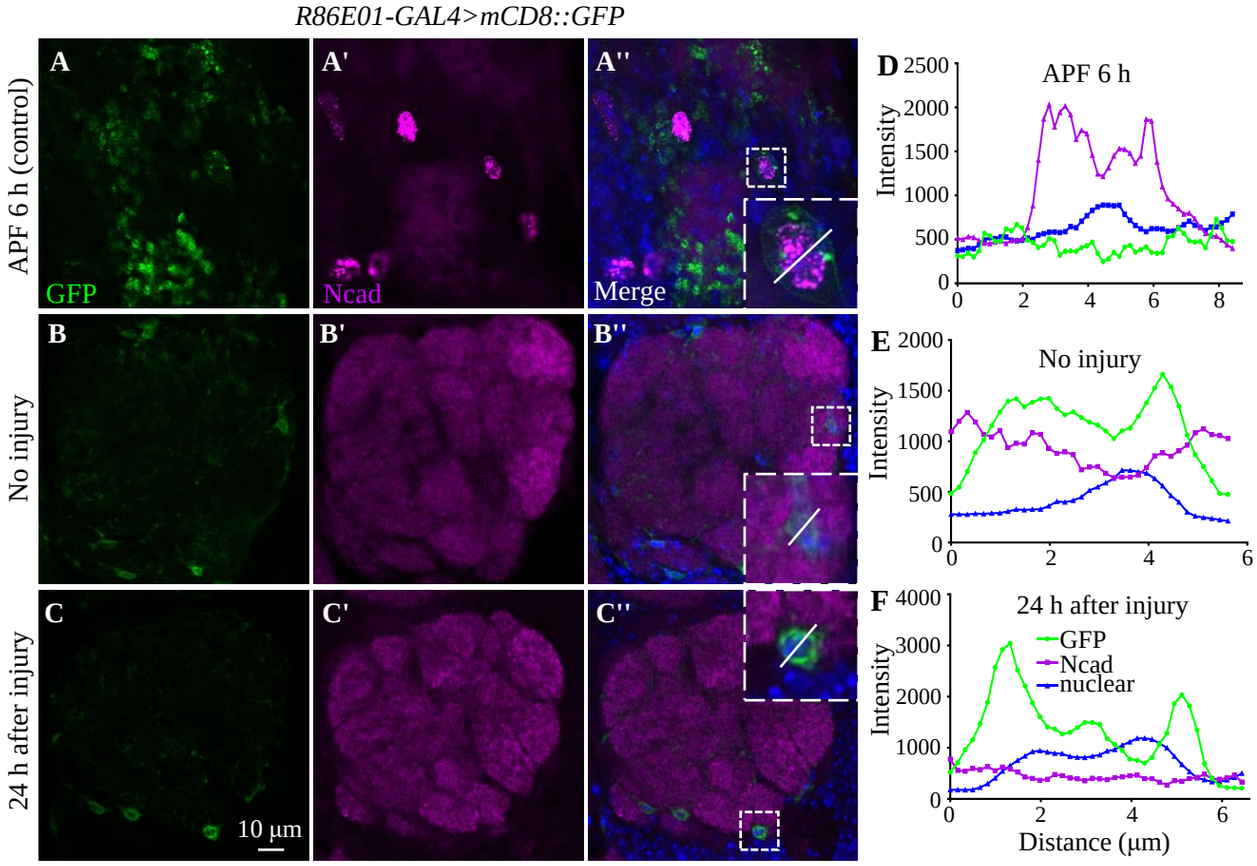
R86E01-GAL4>mCD8::GFP
APF 6 h (control)
No injury
24 h after injury
A
A'
A''
B
B'
B''
C
C'
C''
GFP
Ncad
Merge
10 µm
D
APF 6 h
E
No injury
F
24 h after injury
GFP
Ncad
nuclear
Intensity
Distance (µm)